Dome formation and extension in the Tethyan Himalaya, Leo Pargil, northwest India

Rasmus C. Thiede[†]
Institut für Geowissenschaften, Universität Potsdam, Postfach 601553, Potsdam 14415, Germany

J. Ramón Arrowsmith[‡]
Department of Geological Sciences, Arizona State University, Tempe, Arizona 85287-1404, USA

Bodo Bookhagen[§]
Institut für Geowissenschaften, Universität Potsdam, Postfach 601553, Potsdam 14415, Germany

Michael McWilliams[#]
Geological and Environmental Sciences, Stanford University, Stanford, California 94305-2115, USA

Edward R. Sobel[††]
Manfred R. Strecker[‡‡]
Institut für Geowissenschaften, Universität Potsdam, Postfach 601553, Potsdam 14415, Germany

ABSTRACT

Metamorphic dome complexes occur within the internal structures of the northern Himalaya and southern Tibet. Their origin, deformation, and fault displacement patterns are poorly constrained. We report new field mapping, structural data, and cooling ages from the western flank of the Leo Pargil dome in the northwestern Himalaya in an attempt to characterize its post–middle Miocene structural development. The western flank of the dome is characterized by shallow, west-dipping pervasive foliation and WNW-ESE mineral lineation. Shear-sense indicators demonstrate that it is affected by east-west normal faulting that facilitated exhumation of high-grade metamorphic rocks in a contractional setting. Sustained top-to-northwest normal faulting during exhumation is observed in a progressive transition from ductile to brittle deformation. Garnet and kyanite indicate that the Leo Pargil dome was exhumed from the mid-crust.

$^{40}Ar/^{39}Ar$ mica and apatite fission track (AFT) ages constrain cooling and exhumation pathways from 350 to 60 °C and suggest that the dome cooled in three stages since the middle Miocene. $^{40}Ar/^{39}Ar$ white mica ages of 16–14 Ma suggest a first phase of rapid cooling and provide minimum estimates for the onset of dome exhumation. AFT ages between 10 and 8 Ma suggest that ductile fault displacement had ceased by then, and AFT track-length data from high-elevation samples indicate that the rate of cooling had decreased significantly. We interpret this to indicate decreased fault displacement along the Leo Pargil shear zone and possibly a transition to the Kaurik-Chango normal fault system between 10 and 6 Ma. AFT ages from lower elevations indicate accelerated cooling since the Pliocene that cannot be related to pure fault displacement, and therefore may reflect more pronounced regionally distributed and erosion-driven exhumation.

Keywords: Himalaya, Tibet, extension, dome, geochronology, exhumation.

INTRODUCTION

Within the Himalaya and southern Tibet, the exhumation of high-grade metamorphic domes is a widely distributed tectonic phenomenon (Fig. 1A) that developed since the collision of India and Eurasia in the early Cenozoic (e.g., Gansser, 1964; Molnar and Tapponnier, 1975; Tapponnier and Molnar, 1977; Allegre et al., 1984; Yin and Harrison, 2000). These domes include the Tso Morari of Ladakh (e.g., Berthelsen, 1953; de Sigoyer et al., 2004), the Nanga Parbat and Namche Barwa (Burg et al., 1998; Schneider et al., 1999), the domes of Zanskar (Stephenson et al., 2000; Robyr et al., 2002), the north Himalayan domes (Burg et al., 1984; Chen et al., 1990; Lee et al., 2000, 2004; Watts and Harris, 2005), the domes of the southeastern Karakoram (Maheo et al., 2002), and the Gurla Mandhata (Murphy et al., 2002). Despite their structural similarity, their development is not the result of a single event or process, but rather reflects different stages in the evolution of the Himalayan orogen.

Between Eocene and early Miocene times, the northern Himalaya and southern Tibet underwent multiple phases of north-south–directed crustal shortening (e.g., Ratschbacher et al., 1994; Yin et al., 1994, 1999a), creating topography >5000 m (e.g., Spicer et al., 2003). Since the middle Miocene, regional deformation changed from compression to translation-extension described by a complex and pervasive network of strike slip and normal faults frequently associated with dome formation (see Fig. 1; Molnar and Tapponnier, 1978; Ni and York, 1978; Ni and Barazangi, 1985; Armijo et al., 1986; Coleman and Hodges, 1995; Blisniuk et al., 2001; Taylor et al., 2003; Murphy and Copeland, 2005). Regional structure, tectonic landforms, and seismicity demonstrate that this style of deformation continues today (e.g., Ni and Barazangi, 1984; Molnar and Lyon-Caen, 1989; Fig. 1). The change in deformation caused

[†]E-mail: thiede@geo.uni-potsdam.de.
[‡]E-mail: ramon.arrowsmith@asu.edu.
[§]Present address: Institute for Crustal Studies, University of California, Santa Barbara, California 93106–1100, USA; e-mail: bodo@crustal.ucsb.edu.
[#]E-mail: mcwilliams@stanford.edu.
[††]E-mail: ed@geo.uni-potsdam.de.
[‡‡]E-mail: strecker@geo.uni-potsdam.de.

GSA Bulletin; May/June 2006; v. 118; no. 5/6; p. 635–650; doi: 10.1130/B25872.1; 8 figures; Data Repository item 2006097.

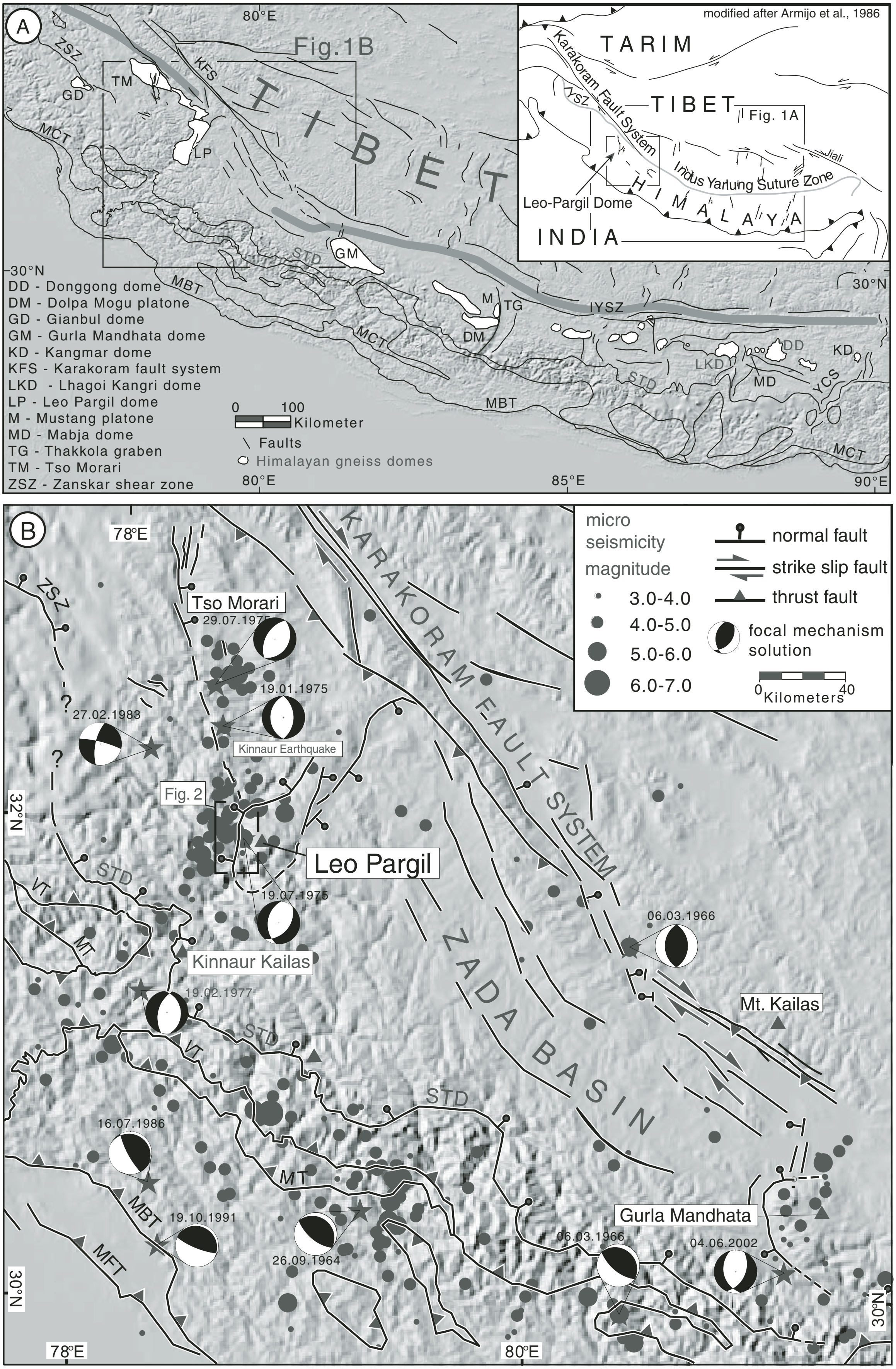
A
80°E
Fig.1B
ZSZ
GD
TM
KFS
TIBET
MCT
LP
STD
GM
30°N
DD - Donggong dome
DM - Dolpa Mogu platone
GD - Gianbul dome
GM - Gurla Mandhata dome
KD - Kangmar dome
KFS - Karakoram fault system
LKD - Lhagoi Kangri dome
LP - Leo Pargil dome
M - Mustang platone
MD - Mabja dome
TG - Thakkola graben
TM - Tso Morari
ZSZ - Zanskar shear zone
MBT
M
TG
IYSZ
DM
MCT
DD
KD
LKD
MD
YCS
0
100
Kilometer
Faults
Himalayan gneiss domes
80°E
85°E
90°E
modified after Armijo et al., 1986
TARIM
Karakoram Fault System
YSZ
TIBET
Fig. 1A
Jiali
Indus Yarlung Suture Zone
HIMALAYA
Leo-Pargil Dome
INDIA
B
78°E
ZSZ
Tso Morari
29.07.1975
19.01.1975
27.02.1983
Kinnaur Earthquake
KARAKORAM FAULT SYSTEM
micro seismicity magnitude
3.0-4.0
4.0-5.0
5.0-6.0
6.0-7.0
normal fault
strike slip fault
thrust fault
focal mechanism solution
0
40
Kilometers
Fig. 2
32°N
Leo Pargil
STD
VT
MT
19.07.1975
06.03.1966
Kinnaur Kailas
19.02.1977
Mt. Kailas
ZADA BASIN
STD
VT
STD
16.07.1986
MT
MBT
19.10.1991
26.09.1964
Gurla Mandhata
06.03.1966
04.06.2002
MFT
30°N
78°E
80°E
30°N

Figure 1. (A) Distribution of high-grade metamorphic domes and major fault systems of the Himalaya and southern Tibet superposed on shaded relief (GTOPO 30 USGS). Fault boundaries are modified in parts A and B after Gansser (1964), Armijo et al. (1986), Hodges (2000), Vannay et al. (2004), and Watts and Harris (2005). High-grade metamorphic domes developed along the entire Himalayan arc, exclusively in the hinterland of the southern Himalayan deformation front. Outlined box indicates the location of part B. (B) Compilation of major faults and microseismicity (circles) of the northwest Himalaya and southern Tibet (NEIC 1977–2004, ISC, Molnar and Lyon-Caen [1989]). Most microseismicity is distributed across the southern Himalayan front. In the hinterland of the Himalaya, microseismicity is limited to the northwest and southeast terminations of the Zada basin. Lower hemisphere diagrams of focal spheres show fault plane solution; open quadrants include compressional P-wave first motion; black quadrants include dilatational first motion. Fault plane solutions indicate larger seismic events associated with compressional fault displacement along the southern Himalayan front and east-west–oriented extensional or strike-slip fault displacement within the hinterland. VT—Vaikrita thrust; MCT—Main Central thrust; MT—Munsiari thrust; MBT—Main Boundary thrust; MFT—Main Frontal thrust; STD—Southern Tibetan detachment system; ZSZ—Zanskar shear zone.

(1) formation of intramontane basins including the Zada basin (Gansser, 1964; Ni and Barazangi, 1985), the Pulan basin (Gansser, 1964; Ni and Barazangi, 1985; Murphy et al., 2002) and several smaller basins along the Karakoram fault system; and (2) the development of north-south–striking grabens within the southern Tibetan Plateau and the High Himalaya (Armijo et al., 1986; Coleman and Hodges, 1995). The question of if and how processes related to this change in deformation style may have influenced widespread tectonic denudation within the Tethyan sedimentary sequence and the exhumation of high-grade metamorphic domes in the High Himalaya is still debated (Gansser, 1964; Murphy et al., 2002; Murphy and Copeland, 2005; Kapp and Guynn, 2004).

Here we describe the development of high-grade metamorphic rocks exposed at the western termination of the Zada or Upper Sutlej basin within the northwest Tethyan Himalaya using detailed structural observations and geochronology. These high-grade rocks describe the Leo Pargil dome, whose ridge line forms the regional topography with Leo Pargil as its highest peak (~6500 m). The high-grade rocks of the Leo Pargil dome are separated from a low-grade metamorphic Tethyan sequence by a narrow transition zone. In the following paragraphs we quantify the deformation of the Leo Pargil dome in space and time to assess the style, magnitude, and origin of dome formation. Within the context of regional extension described previously, we estimate the relative importance of tectonic and erosional exhumation. Our new $^{40}Ar/^{39}Ar$ and apatite fission track (AFT) analyses help to reconstruct the cooling history of the upper crust caused by normal faulting and erosion from temperatures of 450–60 °C. New structural data and regional mapping help us to demonstrate that the formation of the western flank of the Leo Pargil dome was controlled by sustained east-west to ESE-WNW–oriented normal faulting since at least middle Miocene time. The exhumation of the Leo Pargil dome and the neighboring Gurla Mandhata dome (e.g., Murphy et al., 2002) has been controlled by east-west extension, in contrast to older domes such as the Tso Morari dome (e.g., Berthelsen, 1953; de Sigoyer et al., 2004) or the northern Himalayan domes (Burg et al., 1984; Lee et al., 2000), which are characterized by dominantly north-south–oriented extension.

Evolution of the Himalayan-Tibetan Orogen

The Himalayan orogen has four major tectonostratigraphic units: the Tethyan Himalaya, the High Himalayan Crystalline, the Lesser Himalaya, and the Himalayan foreland basin. These are bounded by north-dipping crustal-scale fault systems that include the Main Frontal thrust, the Main Boundary thrust, the Main Central thrust, and the South Tibetan detachment system (e.g., Gansser, 1964; Lefort, 1975; Burg and Chen, 1984; Burchfiel et al., 1992). Between the South Tibetan detachment system to the south and the Indus-Yarlung suture zone to the north (Fig. 1), the Tethyan Himalaya comprises the Lower Proterozoic to Cambrian sediments of the Haimantas Group (Frank et al., 1995) and the Paleozoic–Eocene Tethyan sedimentary sequence associated with the former Indian northern passive margin (e.g., Gansser, 1964; Gaetani and Garzanti, 1991; Steck, 2003).

The Tethyan Himalayan fold-and-thrust belt accommodated crustal shortening and thickening by thin-skinned thrust faults that produced moderate burial with low-grade metamorphic overprint (Steck et al., 1993; Ratschbacher et al., 1994; Frank et al., 1995; Wiesmayr and Grasemann, 2002). Shortening is expressed by southwest-verging folds, northeast-dipping axial surfaces, and schistosity with a northeast-plunging stretching lineation. Compressional deformation is characterized by a top-to-the-SW sense of shear associated with the Eo-Himalayan deformation between 60 and 33 Ma (Hodges and Silverberg, 1988; Wiesmayr and Grasemann, 2002; Steck, 2003). Contemporaneously to the south, underthrusting of the High Himalayan Crystalline was accommodated along the South Tibetan detachment system along the transition between the Tethyan Sedimentary Sequence and the Haimantas Group (Herren, 1987; Wiesmayr and Grasemann, 2002). This resulted in deeper burial, a stronger metamorphic overprint, and partial melting of rocks of the Haimantas Group. The South Tibetan detachment system was reactivated during early to mid-Miocene time along the southwestern termination of the Tethyan Sedimentary Sequence as a major shear zone with normal displacement, facilitating rapid exhumation of the High Himalayan Crystalline to the south (Burg and Chen, 1984; Burchfiel et al., 1992). At the same time, along the northern termination of the Tethyan Sedimentary Sequence, the Great Counter thrust system accommodated north-south shortening (Gansser, 1964; Ratschbacher et al., 1994; Quidelleur et al., 1997; Yin et al., 1999a). South of the intersection between the dextral Karakoram fault and the Indus-Yarlung suture zone, the large intramontane Zada basin was filled with fluvial and lacustrine sediment (Gansser, 1964) (Fig. 1). The Zada basin is bounded by major normal fault systems that separate it from the Gurla Mandhata to the east (Murphy et al., 2002) and the northeast-southwest–oriented Leo Pargil dome to the west (Fig. 1; Hayden, 1904; Ni and Barazangi, 1985).

METHODS

$^{40}Ar/^{39}Ar$ and AFT thermochronology are powerful tools for characterizing the exhumation history and cooling of footwall rocks that accompany normal-fault slip in the brittle crust (e.g., John and Foster, 1993; Ehlers et al., 2001; Armstrong et al., 2003). We studied the western flank of the Leo Pargil dome along a traverse from Sumdo in the north to the confluence of the Spiti-Sutlej Rivers in the south (Figs. 2 and 3). We conducted two WNW-ESE transects, one close to Chango (A–A′, Fig. 4), and a second west of Sumdo (B–B′, Fig. 5). Four $^{40}Ar/^{39}Ar$ mica samples and 14 AFT samples were analyzed. The A–A′ transect was investigated to assess the deformation of

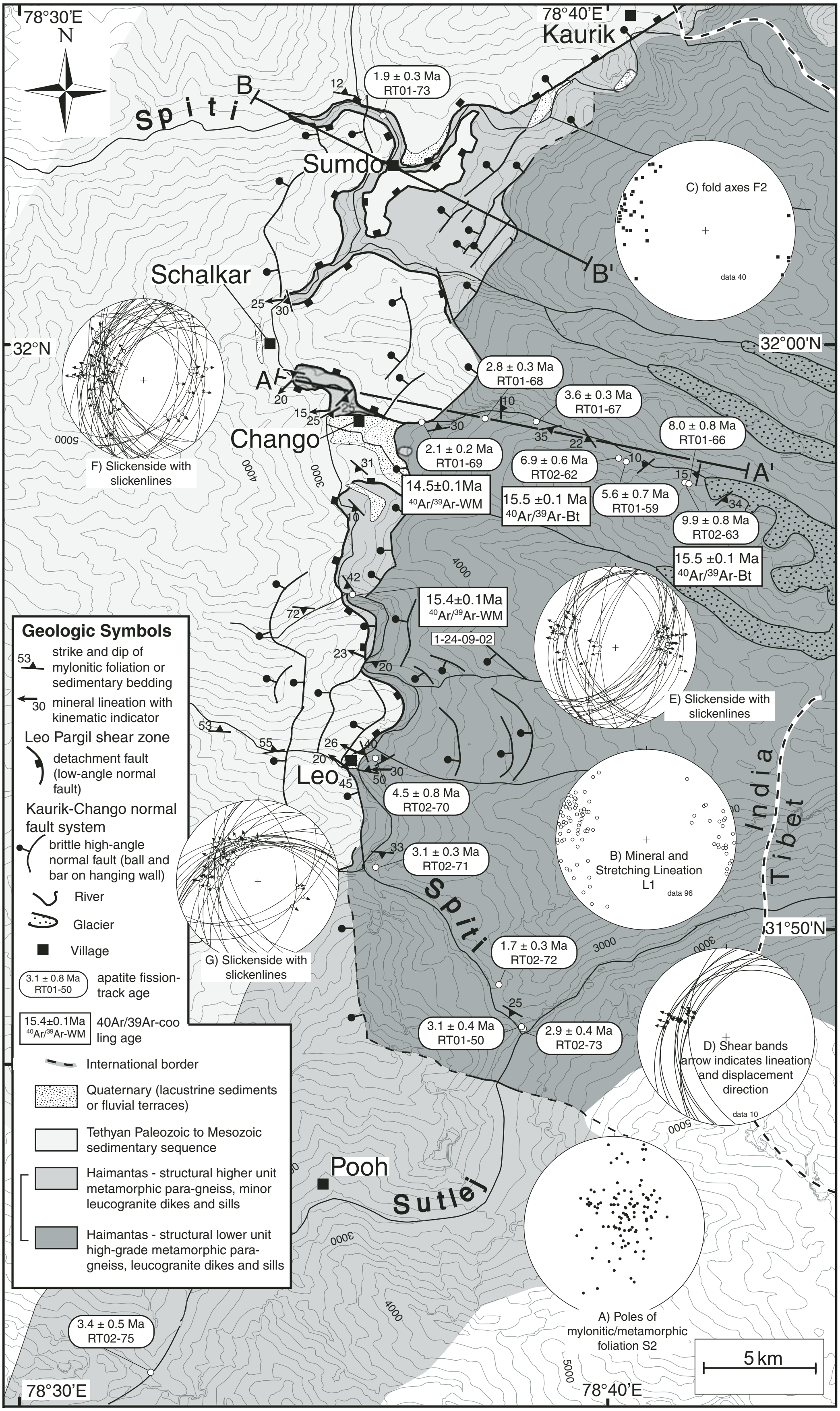

Figure 2. Geologic map of the western flank of the Leo Pargil dome, from field mapping and interpretation of 1:100,000 Landsat™ images. High-grade metamorphic paragneisses that are pervasively intruded by leucogranitic dikes and sills are dark gray. During east-west extension, these high-grade rocks were exhumed along major fault systems such as the Leo Pargil shear zone and the Kaurik-Chango normal fault. Stereoplots (lower hemisphere) show a compilation of all structural data collected across the western flank: (A) poles of mylonitic foliation, S_2; (B) orientation of mineral and stretching lineation, L_2; (C) fold axes, F_2; (D) shear bands; great circles are fault surfaces; arrows indicate displacement directions; (E–G) great circles are slickensides; arrows indicate displacement direction. Ductile and brittle structural data indicate WNW-ESE fault displacement. Transect A–A′ shown in Figure 4; transect B–B′ shown in Figure 5.

the footwall (Figs. 3 and 4), and transect B–B′, the hanging wall (Fig. 5). Both transects are oriented parallel to the mylonitic and mineral stretching lineations and are thus parallel to the dominant displacement direction. The north-south–oriented traverse was designed to constrain fault displacement along strike. If fault slip was rapid and of sufficient displacement, the $^{40}Ar/^{39}Ar$ and AFT thermochronology would constrain the time of cooling and exhumation caused by faulting and erosion.

Low-Temperature Thermochronology

The AFT analyses were conducted to date low-temperature cooling and exhumation within the western flank of the Leo Pargil dome. All samples analyzed (Table DR1[1] and Fig. 2) were collected in fresh outcrops where no alteration was observed. For very young apatites, it may be impossible to obtain a sufficient number of etch-pit figures called *Dpar* (Donelick et al., 1999) for a robust interpretation. However, several samples with older ages and/or higher U content yielded multiple Dpar measurements for most crystals analyzed, allowing us to constrain the closure-temperature range applicable to the composition of the apatites analyzed (Ketcham et al., 1999). With the exception of sample RT01-66, all of the single population ages in this study passed a χ^2 test. Pooled ages are reported with 1σ errors. Three partially annealed AFT ages with a sufficient track-length population along the Chango transect were modeled with the AFTSolve code (ftp://ctlab.geo.utexas.edu/Ketcham/ft/AFTSolve/) (Ketcham et al., 2003) to characterize the exhumation pathway during cooling of the Leo Pargil dome.

$^{40}Ar/^{39}Ar$ analyses of mica were designed to date moderate-temperature cooling and exhumation of the footwall rocks of the Leo Pargil shear zone. Ages and isotopic ratios are reported at a 1σ uncertainty. Samples were step-heated to obtain isochron plots that allow us to measure and correct for the $^{40}Ar/^{36}Ar$ composition of the trapped nonradiogenic argon. Estimated closure temperatures (Dodson, 1973) for ^{40}Ar are ~300–350 °C for biotite (Hodges, 1991, and references therein) and ~350–450 °C for white mica (Purdy and Jaeger, 1976; McDougall and Harrison, 1999, and references therein), depending on the cooling rate and composition.

[1]GSA Data Repository item 2006097, mythological background of the AFT analyses; data table of the fission track results; the inverse isochrones and apparent age spectra of $^{40}Ar/^{39}Ar$ mica analysis; and photograph showing mylonitic rocks referred to the Leo Pargil shear zone, is available on the Web at http://www.geosociety.org/pubs/ft2006.htm. Requests may also be sent to editing@geosociety.org.

LEO PARGIL DOME

The high-grade rocks of the western flank of the Leo Pargil dome are alternating metapelitic schists, phyllites, metasiltstone, metagraywacke, and subordinate quartzites. Most are dark-greenish to brownish quartz-feldspar, mica-garnet gneisses, and mica schists. Their alternating mineral composition and varying grain size suggest a sedimentary protolith, probably a correlative of the Haimantas Group. We therefore refer to these rocks as paragneisses. The high-grade rocks were exhumed from substantial depths, as indicated by the presence of garnet, staurolite, and kyanite. The paragneisses can be divided into two groups, distinguished by sporadic (bright-gray section in Fig. 2) or pervasively distributed intrusions (dark-gray unit in Figs. 2 and 3B). The leucocratic intrusions are centimeter- to meter-scale sills and dikes that constitute between 10% and 50% of the host rock (Fig. 3B–D). White-mica granite, white-mica and tourmaline-bearing granite, two-mica granite, and granite rich in biotite are evident. In the accessible part of the Leo Pargil dome, no major pluton has been detected within its core.

Leo Pargil Shear Zone

The Leo Pargil shear zone divides high-grade metamorphic rocks from the alternating sedimentary rocks of the Tethyan Sedimentary Sequence. Rocks within a several hundred-meter-thick transition zone exposed along the base of the Tethyan Sedimentary Sequence are characterized by a tightly aligned fabric of mica, feldspar, and quartz that form a pervasive WNW-ESE–oriented mineral lineation plunging toward the WNW (Fig. 2, plot B) and a steep subvertical metamorphic gradient. We link this transition zone to a ductile shear zone that bounds the western flank of the Leo Pargil dome (Fig. 4 and 6A). The continuation of the fault trace to the NE and SW is unclear and is inferred from satellite imagery. The Leo Pargil shear zone is several tens to hundreds of meters thick and dips gently to the west. Fine-grained rocks with a strongly developed planar foliation and mineral lineation characterize rock units related to this shear zone. The mylonitic fabric is especially well developed within the quartz- and limestone-rich layers, related to preferred shear horizons at the base of the Tethyan Sedimentary Sequence (see Fig. DR1; see footnote 1).

Rock Types and Structures of the Leo Pargil Shear Zone Footwall

Near Chango (Fig. 6A) the Leo Pargil shear zone is well exposed. On the basis of macroscopic criteria, three main units can be distinguished in the field: (1) dark paragneisses with sporadic intrusions (Fig. 2, light-gray unit; or Fig. 6A, dark rocks forming the footwall of the Leo Pargil shear zone at left), (2) pervasively intruded dark paragneisses (Fig. 2, dark-gray unit of Fig. 3B), and (3) layered low-grade Tethyan Sedimentary Sequence rocks (Hayden, 1904). The consistent rock fabrics and mineral composition indicate that type (1) and (2) paragneisses are probably from the same protolith. Crosscutting relationships suggest four deformation phases, D_1 to D_4 (e.g., Ramsay, 1967; Ramsay and Huber, 1987). Structural features are conventionally delineated with S_i as foliation, L_i as lineation, F_i as folding, and D_i for deformation. Subscripts indicate the relative timing, i.e., lineation L_1 formed during deformation D_1.

In the upper part of transect A–A′ (Fig. 4), the pervasively intruded paragneiss unit was deformed during D_1, forming a dominant, penetrative foliation (S_1) with a mainly subhorizontal and preferentially west-dipping orientation (Fig. 2A). Well-aligned east-west– to WNW-ESE–oriented micas, feldspar, and quartzite grains define a closely spaced mineral lineation, L_1 (Fig. 2B). Occasionally, mylonitic shear zones parallel to the metamorphic fabric, S_1, were observed. The mylonitic foliation, S_1, is folded at micro- and macroscopic scales. Axes of tight to isoclinal F_1 folds are oriented subparallel to the dominant mineral lineation, L_1 (Fig. 2C). Recrystallized feldspar grains indicate at least amphibolite-grade metamorphic conditions during phase D_1. S-C and S-C′ foliations from S_2 are defined by aligned biotite, white mica, and recrystallized quartz grains, indicating top-to-W shear. However, shear indicators, including mantled feldspar porphyroclasts forming δ and σ clasts and stair-stepping relationships (e.g., Hanmer, 1984; Passchier and Simpson, 1986), indicate both top-to-E and -W shear senses. Multiple granitic intrusions and the variable intensity of ductile deformation were observed. Most of the sills are parallel to the S_1 penetrative gneissic foliation as well as the mylonitic shear-zone foliation of the Leo Pargil shear zone (Fig. 3B). Late-stage, virtually undeformed granitic to pegmatitic dikes consisting of coarse feldspars and centimeter-scale white micas cut across the metamorphic fabrics. We interpret these as successive generations of syntectonic intrusions.

During D_2 deformation, the footwall was deformed as ubiquitous millimeter- to meter-scale shear bands cutting across the main S_1 paragneiss foliation (Figs. 2D and 3C). The S_2 shear bands are equally distributed in the upper 2 km of the exposed footwall and indicate pervasive ductile to brittle-ductile deformation. In

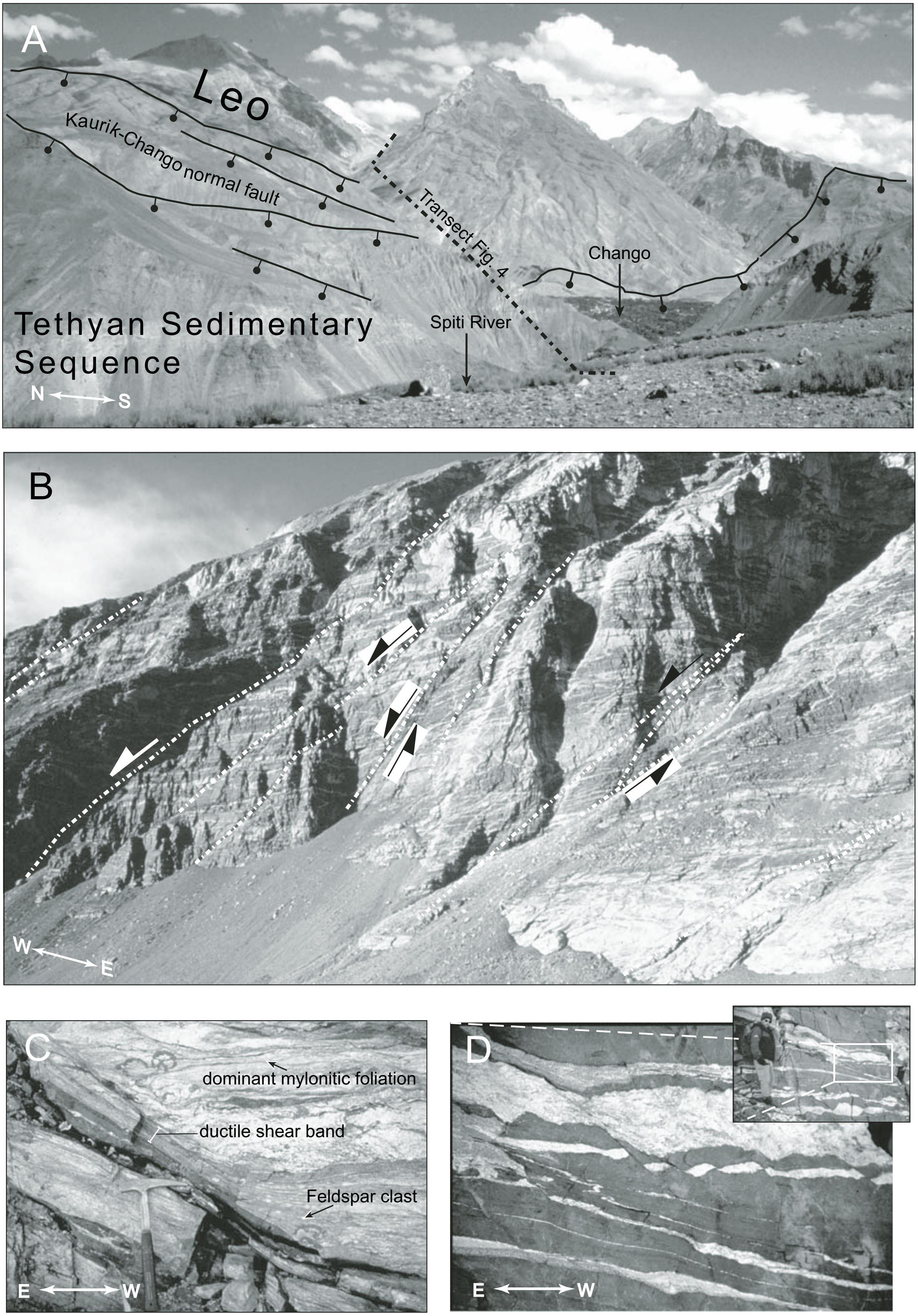
A
Leo
Kaurik-Chango normal fault
Transect Fig. 4
Chango
Spiti River
Tethyan Sedimentary Sequence
N S
B
W E
C
dominant mylonitic foliation
ductile shear band
Feldspar clast
E W
D
E W

Figure 3. (A) View toward east of the Leo Pargil dome from a position west of the Kaurik-Chango normal fault zone. In the background, high-grade metamorphic rocks form the Leo Pargil dome, and the footwall of both the Leo Pargil shear zone and the Kaurik-Chango normal fault. In the foreground are the unmetamorphosed rocks associated with the Tethyan Sedimentary Sequence. (B) Leucocratic dikes and sills have pervasively intruded dark, high-grade metamorphic paragneiss of the Leo Pargil dome, shown as the dark-gray unit in the map in Figure 2. Pervasive, west-dipping faults may be interpreted as Riedel shears of the brittle-ductile stage of the Leo Pargil shear zone. (C) Ductile shear band within high-grade metamorphic paragneiss crosscutting both mylonitic foliation and/or metamorphic layering, indicating top-to-the-west normal displacement. Quartzite shows ductile deformation, whereas feldspar documents brittle deformation, indicating temperatures of ~300 °C during deformation. (D) Metamorphic layering is offset by brittle-ductile faults and/or back rotation by boudinage. Note that feldspar-enriched layers (light) react in a more brittle manner, whereas quartz-rich layers (white) deform in a more ductile manner.

most cases, the paragneisses form low-strain lenses at centimeter to kilometer scales and are surrounded by anastomosing leucogranites. Typically, the quartz-rich layers were deformed in ductile fashion, whereas the feldspars were mainly deformed by brittle fracturing or flow within a quartz-rich matrix (Fig. 3C) indicative of temperatures of ~300 °C during deformation (Linker et al., 1984; Tullis and Yund, 1987). Most shear bands are synthetic to S$_1$ with a penetrative east-west stretching lineation, L$_2$, and reveal normal top-to-the-W sense of shear (Fig. 2D). In addition, the trace of the detachment fault undulates with a kilometer-scale wavelength, and axes are oriented subparallel to the stretching lineation.

The high-grade metamorphic rocks in transect A–A′ (Fig. 4) are characterized by penetrative, west-dipping brittle-ductile D$_3$ (Fig. 3D) and brittle D$_4$ faults. Using granitic sills as offset markers, only minor offset of a few centimeters to meters is observed (Fig. 3B). These faults are synthetic to the shear bands associated with the D$_3$ brittle-ductile stage of the main Leo Pargil shear zone. In addition, conjugate sets of steeply west- and east-dipping faults with steep slickenlines, quartzitic fibers, and bent mylonitic schistosity clearly indicate east-west extension and moderate stretching of the footwall and hanging-wall rocks of the Leo Pargil shear zone during phase D$_4$ (Fig. 2E).

Hanging-Wall Rocks of the Leo Pargil Detachment Fault

The hanging-wall rocks are phyllites, marbles in transition with limestones, quartzites, and sandstones. Only the lowest few hundred meters display a strong mylonitic and metamorphic overprint characterized by the synkinematic growth of micas (Fig. 6). Layers rich in quartz and limestone are completely recrystallized, highly deformed, and thinned, and are characterized by a mylonitic fabric (Fig. 6). It is therefore difficult to associate these layers with their corresponding stratigraphic unit, but their protolith is clearly sedimentary. At the base of the Tethyan Sedimentary Sequence in the Leo Pargil shear zone hanging wall, an abrupt decrease in the intensity of the metamorphic overprint indicates that rocks of the Tethyan Sedimentary Sequence were neither deeply buried nor subjected to strong regional metamorphism. We interpret this thin, metamorphosed, and highly deformed layer of rocks characterizing the base to have formed syntectonically to phase D$_2$ during the contact with hot, high-grade metamorphic footwall rocks of the Leo Pargil shear zone during exhumation. During D$_3$ deformation, west-dipping listric normal faults in transect B–B′ (Fig. 5A) cut hanging-wall rocks of this shear zone at a high angle, were deflected and rotated parallel to the mylonitic fabric, S$_1$, of the footwall rocks (Fig. 5B), and display kilometer-scale open folding perpendicular to the stretching lineation.

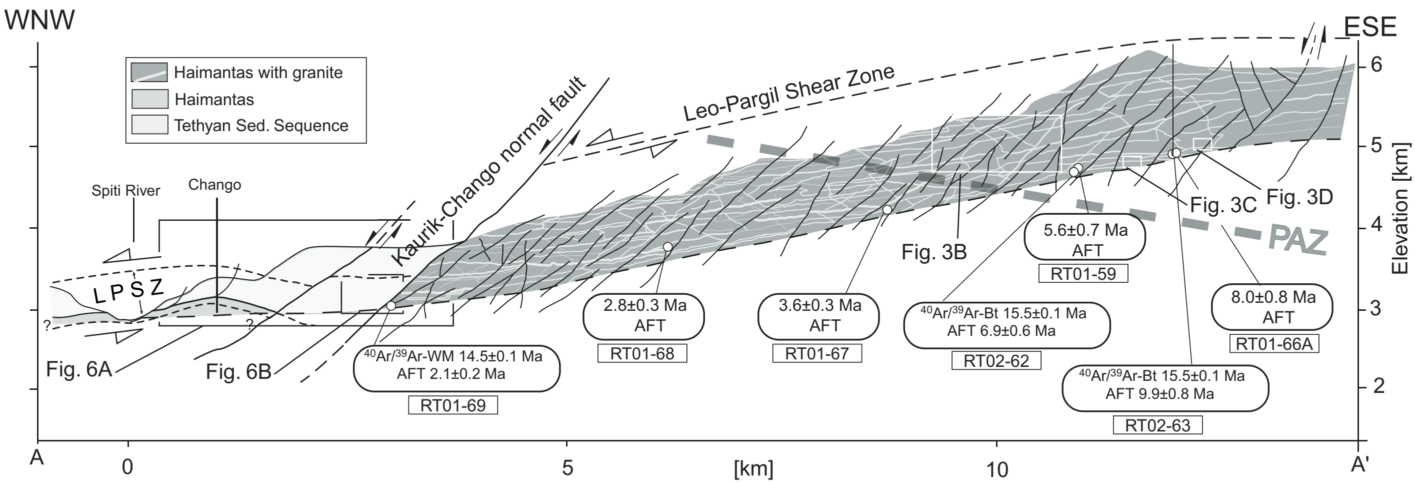

Figure 4. WNW-ESE transect across the western flank of the Leo Pargil dome at the latitude of Chango village (A–A′ in Fig. 2). Apatite fission track (AFT) ages along the transect reveal cooling and extrusion of the high-grade metamorphic footwall rocks of the Leo Pargil detachment fault between 10 and 2 Ma, and young toward the fault (west). ^{40}Ar/^{39}Ar ages indicate regional cooling between 16 and 14 Ma. The extensional shear zone of the Leo Pargil shear zone (LPSZ) is exposed only in the western part of the transect. To the east, the Leo Pargil shear zone has been offset by the Kaurik-Chango normal fault zone. In the footwall of the Kaurik-Chango fault zone, the Leo Pargil shear zone has been removed by erosion, and only a deep structural part of this shear zone is exposed. PAZ—partial annealing zone.

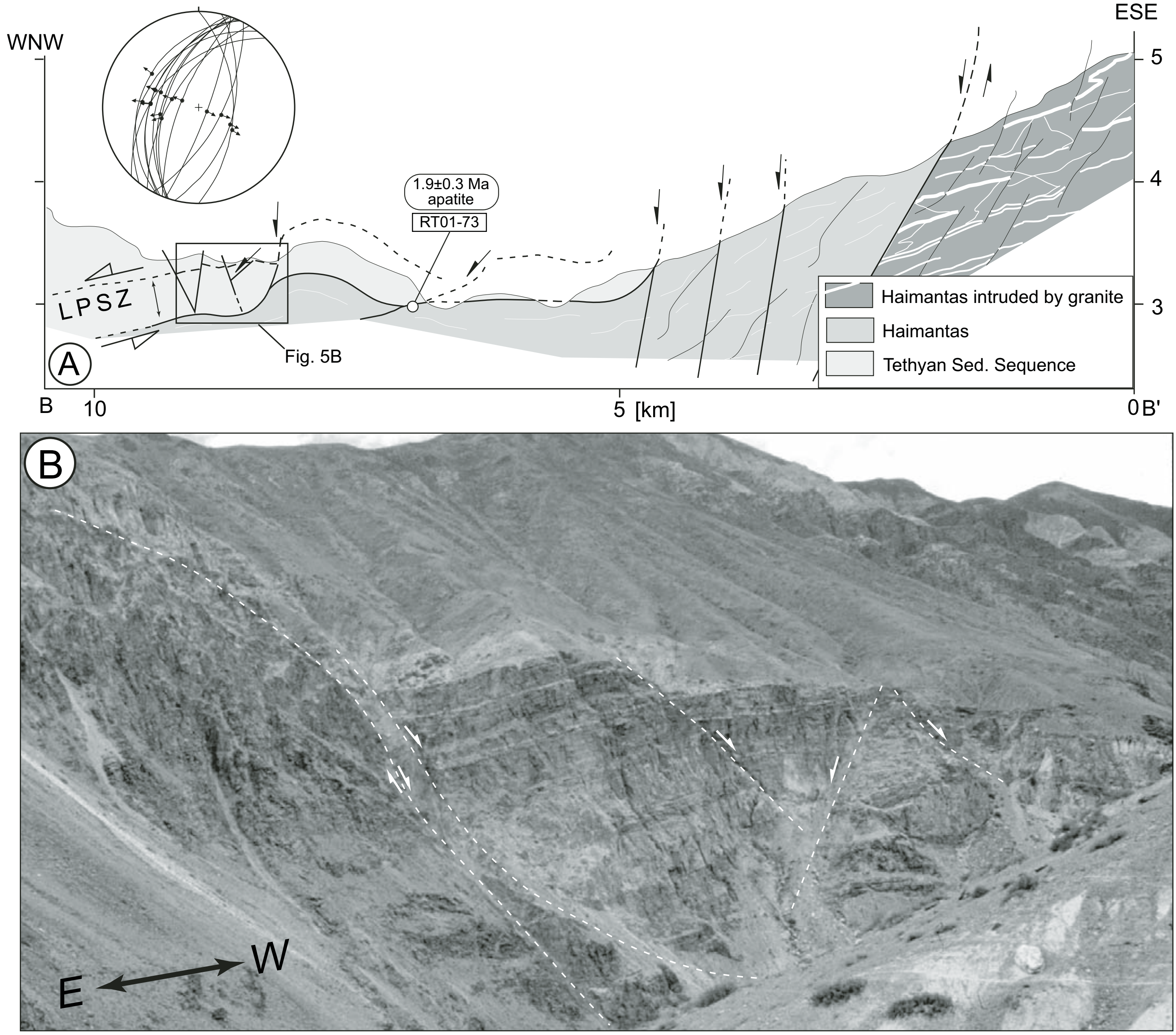

Figure 5. (A) WNW-ESE geologic cross section near Sumdo (B–B′ in Fig. 2) shows the hanging wall of the Leo Pargil shear zone (LPSZ). Listric normal faults cut the hanging wall of this shear zone and sole into its base (see part B), indicating continued east-west extension. Stereonet (lower hemisphere) shows slickensides as great circles with corresponding slickenlines (arrows indicate sense of shear), documenting conjugated high-angle normal fault sets associated with east-west extension. Note that parts A and B of this figure are oppositely oriented. (B) Brittle faulting is present in the detachment hanging wall (see rectangle in A for location). This photo illustrates that the Leo Pargil shear zone was active under brittle-ductile conditions.

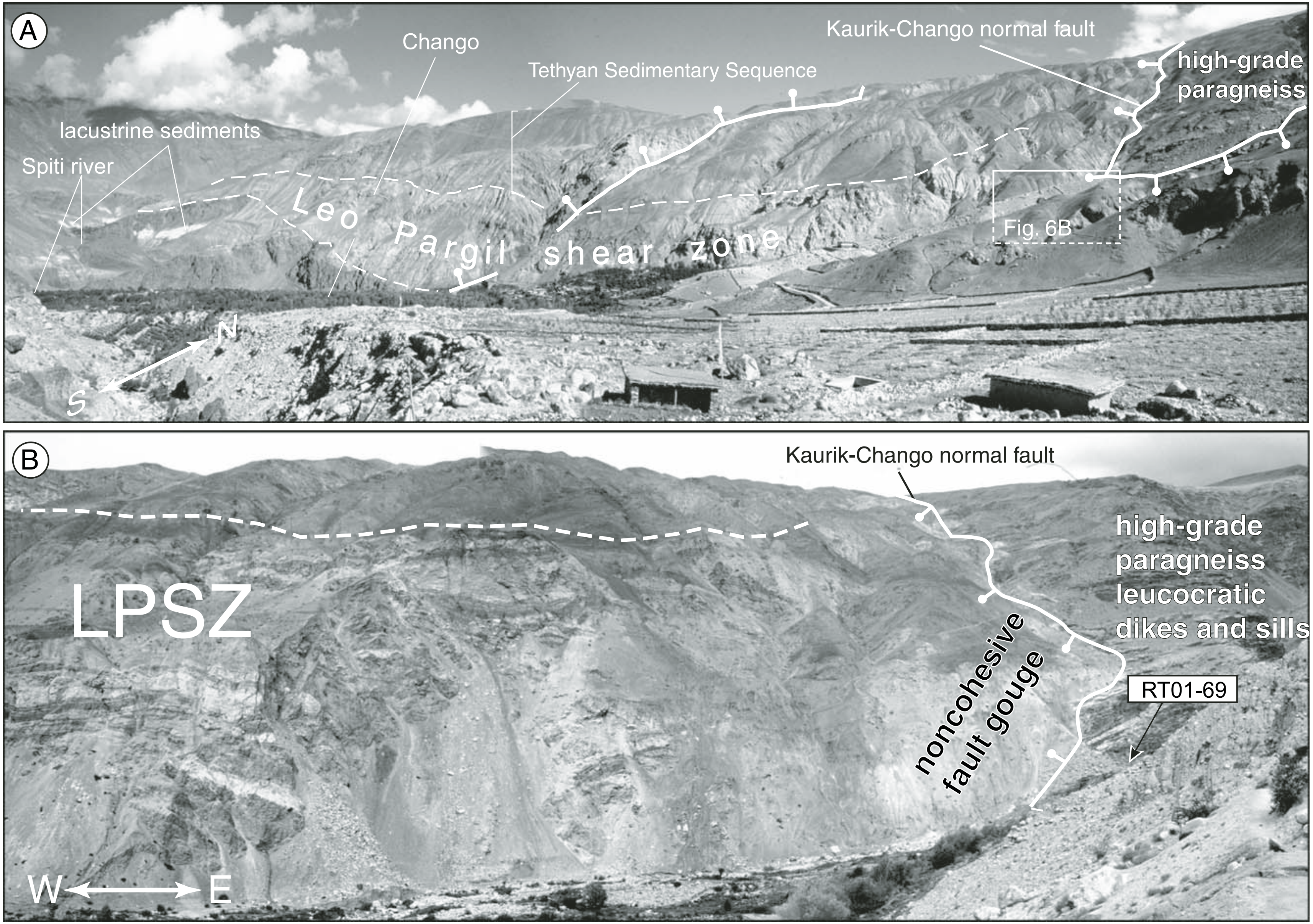

Figure 6. (A) View of the Leo Pargil shear zone (LPSZ) at the contact between the high-grade metamorphic paragneiss (dark rocks) and the base of the Paleozoic section of the Tethyan Sedimentary Sequence (bright cover rocks). Brittle, high-angle normal faults associated with the Kaurik-Chango normal fault zone crosscut the Leo Pargil shear zone. The footwall rocks correspond to deeper segments of the Haimantas Group, which are pervasively intruded by leucocratic dikes and sills, as seen in Figure 3B. Rectangle delineates area of Figure 6B. (B) Eroded noncohesive fault gouge zone of the Kaurik-Chango normal fault zone illustrates its brittle character. On the right side in the hanging wall, the high-grade metamorphic paragneiss is intruded by leucocratic dikes and sills.

Kaurik-Chango Normal Fault Zone

During the final D_4 deformation phase, all structures were cut by north-south–striking, high-angle brittle normal faults that we associate with the Kaurik-Chango normal fault zone (Hayden, 1904). The Kaurik-Chango normal fault zone strikes north-northeast, dips up to 80° to the west (Figs. 3 and 5A), and constitutes a cataclastic fault zone along the western flank of the Leo Pargil dome (Hayden, 1904; Gupta and Kumar, 1975; Bhargava et al., 1978). The faults cut both the hanging-wall and footwall rocks of the Leo Pargil shear zone and are therefore the youngest structures in the area. The hanging wall and footwall of the Kaurik-Chango normal fault expose two different structural levels of the Leo Pargil shear zone. As illustrated in Figure 4, this shear zone itself and rocks associated with Tethyan sedimentary rocks are preserved in the hanging wall. Deeper levels of the Leo Pargil shear zone footwall rocks, characterized by high-grade metamorphic rocks pervasively intruded by leucocratic dikes and sills, form the footwall (Fig. 5). The most prominent strand of the Kaurik-Chango normal fault has created a pronounced topographic break that separates moderately steep slopes in the footwall from steep slopes in the hanging wall (Fig. 3A). Sense-of-slip data collected within this normal fault document WNW-ESE–dipping fault planes (Fig. 2, plots E and F) with steep slickenlines and striations indicating dip-slip normal faulting and east-west extension. Recent tectonic and seismic activity is underscored by transgranular fractures and broken clasts within fluvial fill terraces, the exposure of unconsolidated fault gouge along brittle faults, and faulted lacustrine and fluvial units that are 26–90 ka and contain seismite zones (Singh et al., 1975; Mohindra and Bagati, 1996; Banerjee et al., 1997). Earthquakes and aftershock sequences provide modern insight into active faulting in the Leo Pargil region (Fig. 1B). Focal-mechanism and aftershock studies of the 1975 $\mathbf{M}_b$ 5.8 Kinnaur earthquake (Singh et al., 1975) indicate dominant normal dip-slip displacement (Molnar and Chen, 1983). The epicenter (31.94°N, 078.53°E, ISC) was ~30 km north of the Leo Pargil dome (Fig. 1). The earthquake cluster in Figure 1 is mainly the result of the Kinnaur earthquake aftershocks and defines a NNE-trending seismic zone along the western flank of the dome. This seismically active zone is thus subparallel to the strike of major crustal faults that bound the Leo Pargil dome (Ni and Barazangi, 1985). No hypocenters were recorded along the eastern flank of the Leo Pargil dome. The modern seismicity and young fault scarps suggest that the Kaurik-Chango normal fault is an active feature and is now the main structure controlling tectonic exhumation.

In summary, the juxtaposition of high- and low-grade metamorphic rocks along the Leo Pargil shear zone exposed along the western flank of the Leo Pargil dome resulted from several to tens of kilometers of tectonic displacement. The hanging wall and footwall of this zone have an inventory of common structures such as similarly oriented mylonitic mineral and stretching lineation, sense of shear, and fold-axes that record coeval east-west– to WNW-ESE–directed extension with ductile normal displacement. Isoclinal fold axes and mylonitic lineation with axial fold planes parallel to mylonitic foliation may be related to coaxial thinning during extensional faulting (e.g., Mancktelow and Pavlis, 1994). Top-to-the-west ductile fabrics and brittle east-west extensional faults imply protracted and continuing east-west extension.

THERMOCHRONOLOGY

$^{40}Ar/^{39}Ar$ Thermochronology

Figure 4 summarizes mica $^{40}Ar/^{39}Ar$ and AFT ages from the A–A′ transect across the western flank of the Leo Pargil dome. Two white-mica samples (1-24-09-02 and RT01-69; grain size diameter, ~500 µm) yield flat release spectra with plateau ages of 14.5 ± 0.1 and 15.4 ± 0.1 Ma (Fig. DR2; see footnote 1). Both inverse isochron ages are concordant with the plateau ages when corrected for the presence of excess ^{40}Ar. Sample 1-24-09-02 yields a $^{40}Ar/^{36}Ar$ ratio of 339 ± 11, significantly greater than the atmospheric ratio, and a mean square of weighted deviates (MSWD) of 1.32. While 4 of 17 heating steps define the plateau and its corresponding isochron, they are widely distributed on the 3-isotope plot and define a well-constrained fit. Some apparent ages for the low-temperature steps are suggestive of excess ^{40}Ar. The four-step plateau includes >90% of the total released ^{39}Ar. Sample RT01-69 has a slightly less precise isochron age, because most data cluster close to the $^{39}Ar/^{40}Ar$ axis, resulting in a poorer fit. Excess ^{40}Ar is suggested by the $^{40}Ar/^{36}Ar$ ratio of 684 ± 27; this value is used in computing its plateau age.

Biotite samples RT02-62 and RT02-63, with grain-size diameters between ~200 and 500 µm, yield both well-defined plateau ages of 15.5 ± 0.1 Ma with >75% of the total ^{39}Ar released (Fig. DR2; see footnote 1). Their isochron ages are statistically indistinguishable, using 13 of 17 increments in the regression. In both samples the measured $^{40}Ar/^{36}Ar$ ratio is well constrained and not significantly different from the atmospheric value.

The mica grains we dated are large, and the small difference between their $^{40}Ar/^{39}Ar$ ages suggests rapid cooling through both the white mica and biotite closure temperatures. There is no systematic correlation between age and structural position within the footwall of the Leo Pargil shear zone. We therefore assume that the high-grade core of the Leo Pargil dome cooled homogeneously and rapidly below 300–450 °C between 16 and 14 Ma. We associate the rapid cooling with the emplacement of hot high-grade metamorphic rocks within the upper 10 km of the crust syn- to postdeformational to ductile deformation stage D_2, and syndeformational to stage D_3. These are therefore minimum ages for the onset of rock exhumation.

AFT Thermochronology

Over the entire Leo Pargil dome region we obtained AFT ages between 10 and 2 Ma (Fig. 2 and Table DR1; see footnote 1). Samples collected parallel to transect A–A′ (Fig. 4) yield ages ranging from 9.9 ± 0.8 to 8.0 ± 0.8 Ma (RT02-63 and RT01-66), at high elevation to the east, to 2.1 ± 0.2 Ma (RT01-69), close to the Spiti River in the west. The apparent ages and track lengths plotted with respect to structural level exhibit a characteristic pattern. AFT ages are systematically older, and average track lengths are shorter, with increasing distance from the Kaurik-Chango normal fault and with increasing elevation (Fig. 7).

Samples RT02-62 and -63 and RT01-66 and -67 from high elevation provide important constraints for the exhumation and cooling pathway of the Leo Pargil dome during Mio-Pliocene time. AFT ages between 10 and 8 Ma from the two highest samples (Figs. 4 and 7B) indicate that ductile displacement on the Leo Pargil shear zone and within the high-grade metamorphic rocks had ceased by that time. Owing to a high U content and older cooling ages, these are the only samples that yield representative track-length populations. Samples RT02-62 and -63 have a moderately shortened mean track-length distribution of 13.9 ± 0.2 and 13.1 ± 0.3 µm (Fig. 8), respectively. Sample RT01-67 yields longer mean track lengths of 14.3 ± 0.2 µm. Progressively shorter mean track lengths with increasing elevation indicate increasing annealing, which suggests that samples RT02-62 and -63 may have resided longer within the paleo-partial annealing zone (PAZ) prior to exhumation than samples at lower crustal positions. This is confirmed by sample RT01-67 from a lower part of the Leo Pargil shear zone, which has only a few moderately annealed tracks, indicating that it remained at temperatures high enough to be continuously reset until exhumation began

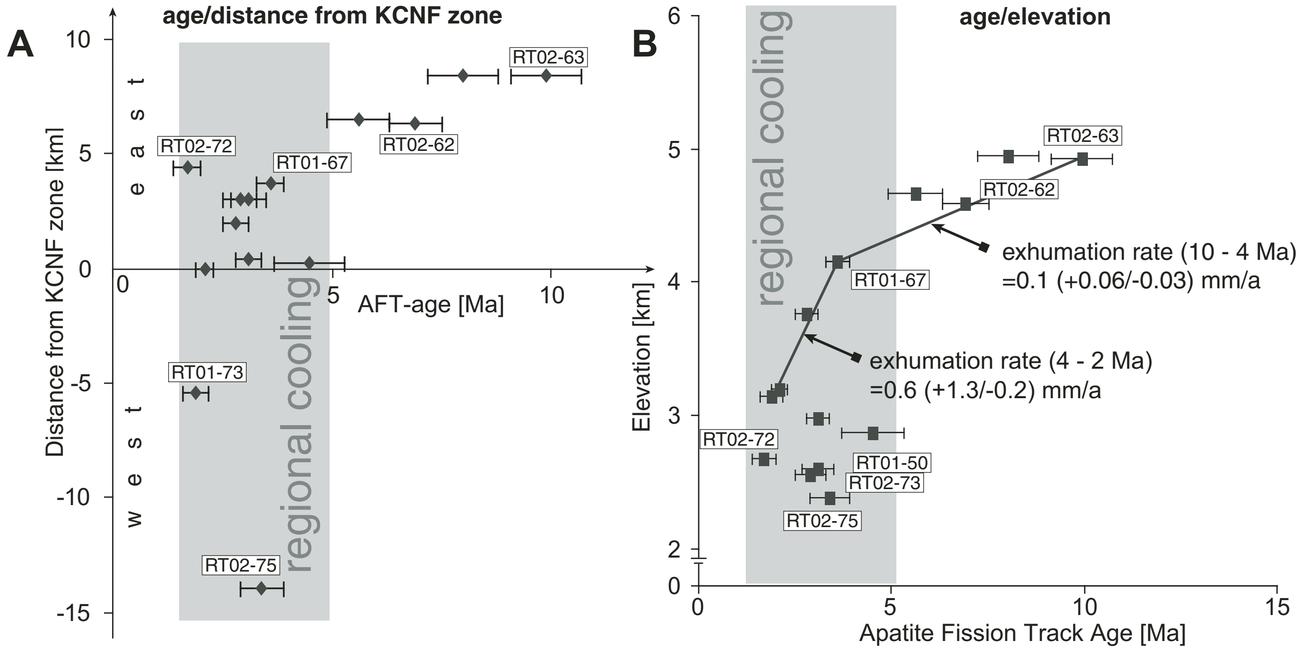

Figure 7. Apatite fission track (AFT) ages plotted (A) versus horizontal distance perpendicular to the Kaurik-Chango normal fault (KCNF), with positive values reckoned eastward, and (B) versus elevation. AFT ages within the gray sector are between 5 and 2 Ma and are independent of the distance to the Kaurik-Chango fault zone and elevation, respectively, indicating regional cooling rather than cooling related to tectonic denudation.

at ca. 4 Ma. The base of the paleo-PAZ is therefore somewhere between samples RT01-67 and RT02-62 (Fig. 4). Moreover, all samples collected below the paleo-PAZ yield cooling ages <4 Ma, indicating that these rocks cooled rapidly from ~120 to 60 °C between 4 and 2 Ma.

This interpretation is consistent with thermal modeling by AFTSolve (Ketcham et al., 2003). Using data from samples RT02-62, -63, and RT01-67, modeling suggests relatively slow to moderate cooling between 5 and 19 °C/m.y. during the late Miocene, followed by more rapid cooling between 20 and 35 °C/m.y. during Pliocene–Quaternary time (Fig. 8). The first cooling phase may be associated with localized tectonic exhumation and brittle deformation along the Kaurik-Chango normal fault during deformation stage D_4 in late Miocene time, followed by more rapid regional cooling and exhumation during the Pliocene–Quaternary.

The lack of unambiguous geologic offsets makes it difficult to further assess the normal-fault displacement rates across the Leo Pargil fault zone. A first order estimate of exhumation rate can be derived from the change in time and space of the AFT results, assuming that the samples were exposed approximately at the same structural level. This estimate is based on the ages of better-constrained samples RT02-62 and -63. The footwall block of the Leo Pargil shear zone accommodated brittle stage exhumation between 10 and 2 Ma, with vertical exhumation rates of ~0.1 (+0.06/–0.03) mm/yr between 10 and 4 Ma, derived from the upper three samples (RT02-63, -62, RT01-67). In contrast, the age-elevation relationship, on the basis of the lower three samples (RT01-67, -68, -69; see Fig. 7B), show faster exhumation rates of ~0.6 (+1.3/–0.2) mm/yr between 4 and 2 Ma.

Lower Spiti Valley Traverse

Seven AFT ages between 4.5 ± 0.8 and 1.7 ± 0.3 Ma (Fig. 2 and Table DR1; see footnote 1) were obtained from hanging-wall and footwall rocks of the Kaurik-Chango normal fault along the north-south segment of the lower Spiti River. The hanging-wall samples (RT01-73 and RT02-75) have ages of 3.4 ± 0.5 and 1.9 ± 0.3 Ma, whereas the footwall samples (RT02-70, -71, -72, -73, and RT01-50) are between 4.5 ± 0.8 and 1.7 ± 0.3 Ma. The AFT cooling ages indicate coeval cooling of both Kaurik-Chango hanging-wall and footwall rocks during the Pliocene and Quaternary. We assume that this normal fault has an untilted fault plane within the upper 3–4 km of the crust, and low to moderate stretching of both the hanging wall and footwall. This limits any displacement along the fault to <3 km. These data show no correlation between age and distance to the Kaurik-Chango normal fault (Fig. 7A) nor between age and elevation (Fig. 7B). Consequently, the observed increase in cooling rates between 4 and 2 Ma may be regional and not associated with displacement along this fault. The inception of Kaurik-Chango faulting may have been established as early as 10–4 Ma, assuming very low displacement rates <0.3 ± 0.1 mm/yr, implying that the bulk of tectonic denudation along the western flank of the Leo Pargil dome was accommodated by the Leo Pargil shear zone before the late Miocene.

In summary, our new thermochronologic data record at least three exhumation stages in the Leo Pargil dome: rapid cooling between 16 and 14 Ma ($^{40}Ar/^{39}Ar$ mica data), cooling and exhumation at a reduced rate between 10 and 4 Ma, and accelerated cooling and exhumation after 4 Ma.

DISCUSSION

We now discuss the tectonic development of the western flank of the Leo Pargil dome and link the three thermochronologic and exhumation phases to the relative chronology of deformation phases D_1 to D_4, documented by the structural data. Pliocene to Quaternary AFT cooling patterns potentially indicate that the youngest phase of exhumation was driven by

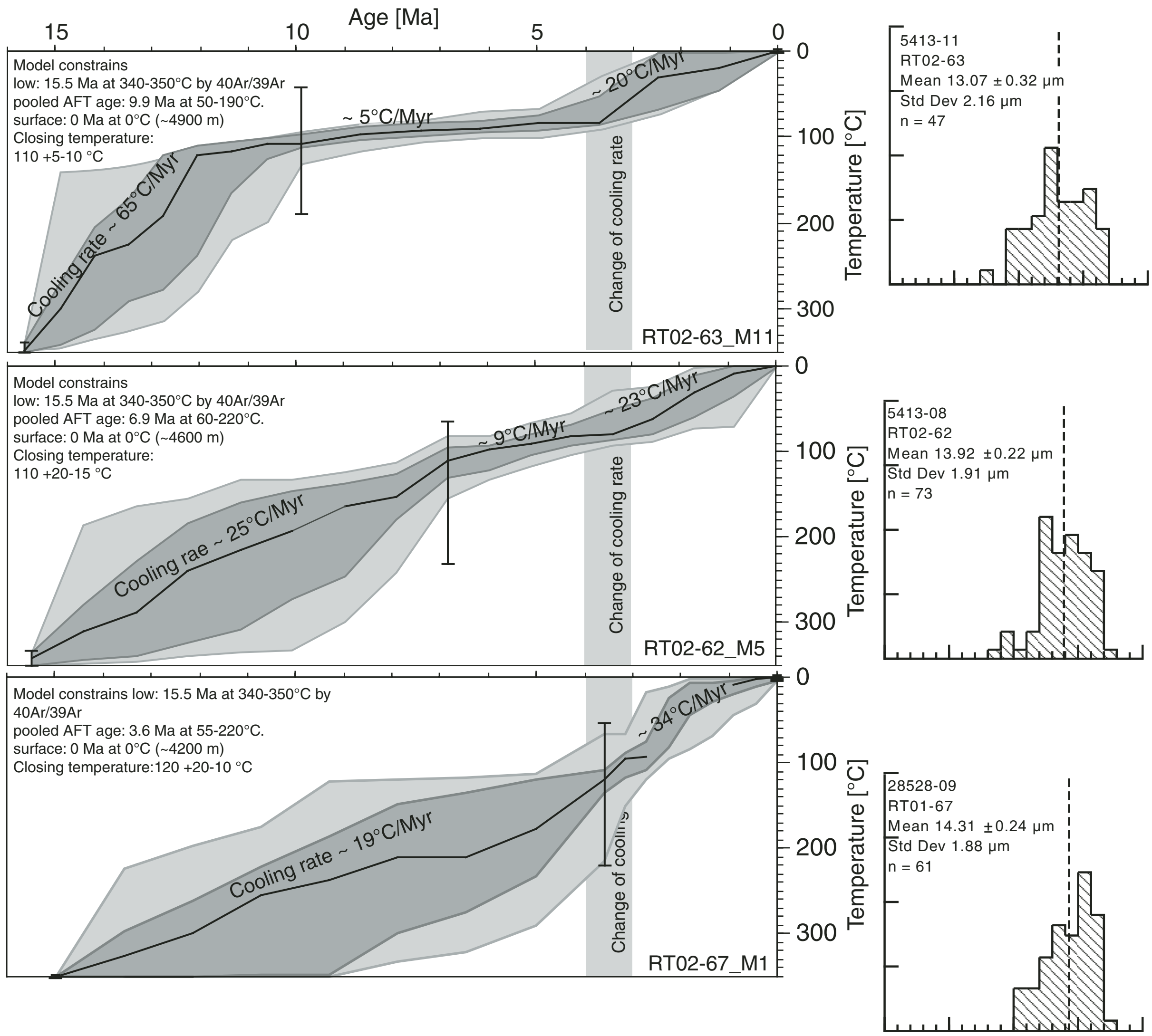

Figure 8. Time-temperature modeling results obtained with AFTSolve (ftp://ctlab.geo.utexas.edu/Ketcham/ft/AFTSolve/; Ketcham et al., 2003) and track-length population. The black line indicates the best-fit time-temperature path, the dark-gray envelope bounds all results with good fit, and the light-gray area with acceptable fit. Note the consistent increase in cooling rate between 4 and 3 Ma for all samples. Cooling path for temperatures higher than Ta are constrained only by Ar ages. The "inverse modeling constrained random search" with 10,000 calculated paths was used. Individual model constraints are given in the text.

erosion and not tectonic faulting. We discuss regional observations related to the Leo Pargil shear zone that indicate that it records a long deformation history and existed prior to dome formation. Finally, we discuss the magnitude of displacement along the western flank of Leo Pargil in relation to the regional tectonic setting, and consider it with respect to models that involve east-west extension in the northern Himalaya and southern Tibet.

Tectonic and Erosional Exhumation

There is an orogen-wide dichotomy of AFT ages in the Himalaya and southern Tibet. Young AFT ages (<ca. 5 Ma) characterize the southern Himalayan front, where rapid exhumation coincides with deep-seated erosion in humid sectors of the orogen (summarized in Thiede et al., 2004). Tibet and the highly elevated, arid portions of the Himalaya generally appear to be characterized by relatively old AFT ages indicative of moderate to slow exhumation (e.g., Kumar et al., 1995; Schlup et al., 2003). Spatially limited middle Miocene to recent ages record fast exhumation along extensional structures such as the Leo Pargil and Gurla Mandhata domes (Murphy et al., 2002) and the north-south–striking Yangbajain graben close to Lhasa and other extensional structures (Pan et al., 1993).

Rapid cooling along the western flank of the Leo Pargil dome may be associated with ductile displacement along the Leo Pargil shear zone during deformation stage D_2 under greenschist metamorphic conditions. The middle Miocene $^{40}Ar/^{39}Ar$ mica data constrain cooling to have occurred during the late syn- to post-D_2 deformation stage. The late Miocene phase of slow cooling and exhumation, on the basis of the AFT results, characterizes a brittle deformation stage that may have been associated with D_4 deformation. Temporal constraints of D_1 and D_3 are approximated relative to D_2 and D_4.

The brittle faults, tectonic geomorphology, and active seismicity all indicate continued fault slip along the Kaurik-Chango normal fault and related structures. Accelerated Pliocene–Quaternary cooling cannot be attributed to the fault displacement along this fault within the resolution of the AFT method. Alternatively, accelerated cooling may have resulted from increased regional erosion associated with faster river incision and/or accelerated propagation of fluvial incision into the watersheds and onto the flanks of the Leo Pargil dome during the last 4 m.y. The timing of accelerated exhumation is intriguing within the context of global climate change, coincident shifts in erosion rates, and the resulting impact on orogenic systems, beginning at ca. 4 Ma (e.g., Qiang et al., 2001; Zhang et al., 2001). Alternatively, an increase in orogen-wide erosion and/or the effects of establishment of a new, more effective river network, such as the Sutlej, may have triggered the regional accelerated cooling pattern. River captures by headwater erosion may be the agent of a sudden lowering of fluvial base level that released a pulse of increased river incision and may also have been coupled with an increase in relief. In contrast, the preservation of two cooling phases within the ATF data collected at high elevation (samples RT02-62 and RT02-63) indicates that younger exhumation and/or erosion has not been deep seated enough to remove all cover rocks that preserve the older history of the internal parts of the Leo Pargil dome. Consequently, these data suggest that either glacial or fluvial erosion during Pliocene to Quaternary time was limited, and <2–3 km of rocks were removed from above Leo Pargil.

Is the Leo Pargil Shear Zone a Reactivated Shear Zone?

Pre-collisional palinspastic reconstructions of the Indian passive margin in the northwest Himalaya reveal that a basal detachment for the Tethyan Sedimentary Sequence probably formed along the rheologic interface between the Tethyan Sedimentary Sequence and the Early Proterozoic–Cambrian Haimantas Group sediments (Wiesmayr and Grasemann, 2002). The stratigraphic relations reported here show that the contact may also be exposed along the Leo Pargil dome. If so, the Leo Pargil shear zone may form the basal detachment of Eo-Himalayan crustal shortening (Fig. 4), an interpretation that is consistent with observations of Chen et al. (1990) and Murphy et al. (2002), who documented an equivalent detachment shear zone bounding Gurla Mandhata. They also interpret the basal detachment as a segment of the South Tibetan detachment system exhumed during doming. Thus the Leo Pargil shear zone may have first developed as a contractional, SW-vergent structure during Eo-Himalayan crustal shortening, which was later reactivated during the extrusion of the High Himalayan Crystalline along the South Tibetan detachment system during the early Miocene (Grujic et al., 1996; Nelson et al., 1996). In this scenario, the Leo Pargil shear zone may be not only related to the exhumation of the high-grade metamorphic rocks during dome formation, but it may also represent a long-lasting structure that was multiply reactivated (Wiesmayr and Grasemann, 2002). This assessment is consistent with inferences made for the Zanskar shear zone as a segment of the South Tibetan detachment system in the northwest Himalaya (Herren, 1987; Dezes et al., 1999; Steck, 2003, and references therein).

Regional Displacement Pattern—A Transition from North-South Shortening to East-West–Oriented Extension and Dome Formation

As a consequence of crustal shortening during collision, thickened continental crust is heated and weakened (England and Richardson, 1977; England and Thompson, 1984), affecting orogen-scale deformation processes and forming partially molten crust (Nelson et al., 1996). Partially melted crust may flow laterally to aid in the construction of an orogenic plateau (Royden, 1996) and/or may cause a gravitational (Royden and Burchfiel, 1987; Rey et al., 2001) or orogenic (Vanderhaeghe et al., 1999) collapse coupled with extension. Many intramontane sectors of major orogens are characterized by normal and strike-slip faulting, intramontane basins, and domal structures that led to significant tectonic denudation and exhumation of high-grade metamorphic rocks already during syncollisional contraction (e.g., Lee et al., 2000; Robyr et al., 2002; de Sigoyer et al., 2004; Lee et al., 2004).

Within the Himalayan orogen, Eocene to early Miocene northeast-southwest–oriented crustal shortening (Ratschbacher et al., 1994; Yin et al., 1994; Quidelleur et al., 1997; Yin et al., 1999b) was superseded by east-west–oriented upper crustal extension (Ratschbacher et al., 1994; Yin et al., 1994; Coleman and Hodges, 1995; Searle et al., 1998; Yin et al., 1999b), manifested by the localized formation of north-south–oriented grabens (Armijo et al., 1986). The observed transition of the internal strain from north-south shortening to east-west extension may have been caused by a regional reorientation of the tectonic stress field in which σ_1 became vertical, and σ_3 horizontal and east-west oriented. As a result of this reorganization, older domes developed by a dominantly north-south–oriented shortening regime (Burg et al., 1984; Lee et al., 2000), whereas younger domes, such as the Leo Pargil and Gurla Mandhata, appear to have heralded a neotectonic phase of east-west extension. Interestingly, this reorientation is not only consistent with temporal variations in the preferred orientation of dome formation but is also documented within the displacement patterns along the Karakoram fault system. For example, Searle et al. (1998) proposed two periods of rapid cooling along the central parts of the Karakoram fault system, with transpressional fault motion at 18–11.3 Ma, and sustained transtension from 11.3 Ma onward. This is consistent with new Ar/Ar K-feldspar data from this region, revealing accelerated cooling in a transtensional setting between 14 and 10 Ma (Lacassin et al., 2004; Phillips et al., 2004).

Further, the greater Leo Pargil region is characterized by young, north-south–striking, brittle high-angle normal faults, including the Tso Morari normal fault (Berthelsen, 1953; Steck et al., 1998) and normal faults west of Tso Kar (Fuchs and Linner, 1996) that cut all other structures. The NNE-SSW–striking and WNW-dipping Yurda normal fault between the Kashmir basin to the west and the Zanskar crystalline and Kishtwar domes to the east were described by Fuchs (1975), whereas Steck et al. (1998) described the NNE-SSW– and NNW-SSE–striking Kiagor Tso conjugate normal faults. These structures are consistent with those observed in the grabens of southern Tibet (e.g., Armijo et al., 1986; Coleman and Hodges, 1995) and with recent earthquake focal-mechanism solutions from the Tethyan Himalaya and southern Tibet that define shallow events restricted to the overriding Himalayan plate and indicate strike-slip and normal east-west displacement. In contrast, Lee et al. (2000) concluded that formation of the Kangmar dome of southern Tibet resulted from the development of an antiform above a north-dipping ramp along the Gyirong-Kangmar thrust fault system and suggested that this is consistent with the development of other north Himalayan domes. Extension along the Leo Pargil has also been associated with an oblique thrust ramp as suggested by Dubey and Bhakuni (2004), but the rather pervasive and regional character of east-west extension (as documented higher in the section) makes it unlikely that extension in this region is the result of such a structure.

Models Explaining Regional Extension within Northern Himalaya and Southern Tibet

One model that explains regional extension in the Himalaya and adjacent regions is related to gravitational instability of the Tibetan Plateau during the middle Miocene (Molnar and Tapponnier, 1978; Molnar and Chen, 1983;

Coleman and Hodges, 1995). In another model, normal faulting may be caused by processes associated with slab break-off (Chemenda et al., 2000; Maheo et al., 2002) or right-lateral oblique convergence with slip partitioning (McCaffrey and Nabelek, 1998). In still another model, differential eastward extrusion of central and northern Tibet relative to southern Tibet is accommodated by right-lateral motion of the Karakoram-Jiali fault zone and normal faulting (Armijo et al., 1986). In the Leo Pargil region, extension is approximately arc-parallel, and normal faults have evolved perpendicular to the arc of the orogen, consistent with models incorporating oroclinal bending (Klootwijk et al., 1985; Ratschbacher et al., 1994; Bendick and Bilham, 2001).

CONCLUSIONS

Normal faulting in the western flank of the Leo Pargil dome has occurred since the middle Miocene. This deformation accommodates continued exhumation of high-grade metamorphic rocks that form the Leo Pargil dome within the overall tectonic context of a contractional orogen. Sustained east-west extension produced a progressive transition from ductile to brittle deformation during top-to-the-WNW normal displacement. Rocks of the dome contain garnet and kyanite, indicating that they were exhumed from midcrustal levels. The structural patterns of dome formation are consistent with reorganization of the upper crustal strain field within an intramontane part of the Himalaya during the middle Miocene.

New ^{40}Ar/^{39}Ar mica and AFT ages record a three-stage cooling and exhumation pathway from 350–60 °C since the middle Miocene. ^{40}Ar/^{39}Ar mica ages of 16–14 Ma indicate a phase of rapid cooling and may set a minimum age for the onset of dome exhumation. AFT ages of 10 to 8 Ma indicate that D_2 ductile fault displacement must have ceased by then. Track length distributions from samples collected at high elevations suggest that cooling rates had decreased significantly by this time, possibly related to decreased fault displacement along the Leo Pargil shear zone and a possible transition to the Kaurik-Chango normal fault system between 10 and 4 Ma. AFT data from samples at lower elevations document a return to accelerated regional cooling since the Pliocene. This cooling is not related to pure fault displacement but may reflect more pronounced, regionally distributed, and erosion-driven exhumation potentially forced by monsoonal strengthening and/or rapid fluvial incision owing to the Pliocene establishment of a new river network, such as the modern Sutlej River.

ACKNOWLEDGMENTS

The authors would like to thank A.K. Jain and S. Singh for valuable discussions and logistical support, and the great Indian mountain guides S. Slathia and T. Tsering for support during field work. We are grateful to J. Lee for reviewing an earlier version of this manuscript, and A. Carter, M. Murphy, and Associate Editor M. Edwards for thorough, constructive reviews. We thank the Deutsche Forschungsgemeinschaft (DFG) for financial support (grant STR-11/4), and the German Academic Exchange Service (DAAD) for support of R.T. while visiting Arizona State University.

REFERENCES CITED

Allegre, C.J., Courtillot, V., Tapponnier, P., Hirn, A., Mattauer, M., Coulon, C., Jaeger, J.J., Achache, J., Scharer, U., Marcoux, J., Burg, J.P., Girardeau, J., Armijo, R., Gariepy, C., Gopel, C., Li, T.D., Xiao, X.C., Chang, C.F., Li, G.Q., Lin, B.Y., Teng, J.W., Wang, N.W., Chen, G.M., Han, T.L., Wang, X.B., Den, W.M., Sheng, H.B., Cao, Y.G., Zhou, J., Qiu, H.R., Bao, P.S., Wang, S.C., Wang, B.X., Zhou, Y.X., and Ronghua, X., 1984, Structure and evolution of the Himalaya-Tibet Orogenic Belt: Nature, v. 307, p. 17–22, doi: 10.1038/307017a0.

Armijo, R., Tapponnier, P., Mercier, J.L., and Han, T.L., 1986, Quaternary extension in Southern Tibet—Field observations and tectonic implications: Journal of Geophysical Research, v. 91, p. 13,803–13,872.

Armstrong, P.A., Ehlers, T.A., Chapman, D.S., Farley, K.A., and Kamp, P.J.J., 2003, Exhumation of the central Wasatch Mountains, Utah: 1, Patterns and timing of exhumation deduced from low-temperature thermochronology data: Journal of Geophysical Research—Solid Earth, v. 108, no. B3, 2172, p. 1–17.

Banerjee, D., Singhvi, A.K., Bagati, T.N., and Mohindra, R., 1997, Luminescence chronology of seismites at Sumdo (Spiti valley) near Kaurik-Chango Fault, Northwestern Himalaya: Current Science, v. 73, p. 276–281.

Bendick, R., and Bilham, R., 2001, How perfect is the Himalayan arc?: Geology, v. 29, p. 791–794, doi: 10.1130/0091-7613(2001)029<0791:HPITHA>2.0.CO;2.

Berthelsen, A., 1953, On the geology of the Rupshu district, N.W. Himalaya: Contribution to the problem of the central gneisses: Bulletin of the Geological Society of Denmark (Meddelelser fra Dansk Geologisk Forening), v. 12, p. 350–414.

Bhargava, O.N., Ameta, S.S., Gaur, R.K., Kumar, S., Agarwal, A.N., Jalote, P.M., and Sadhu, M.L., 1978, The Kinnaur (H.P., India) earthquake of 19 January, 1975: Summary of geoseismological observations: Bulletin of the Indian Geological Association, v. 11, p. 39–53.

Blisniuk, P.M., Hacker, B.R., Glodny, J., Ratschbacher, L., Bi, S.W., Wu, Z.H., McWilliams, M.O., and Calvert, A., 2001, Normal faulting in central Tibet since at least 13.5 Myr ago: Nature, v. 412, p. 628–632, doi: 10.1038/35088045.

Burchfiel, B.D., Zhileng, C., Hodges, K.V., Yuping, L., Royden, L.H., Changrong, D., and Jiene, X., 1992, The South Tibetan detachment system, Himalayan orogen: Extension contemporaneous with and parallel to shortening in a collisional mountain belt: Geological Society of America Special Paper 269, p. 1–41.

Burg, J.P., and Chen, G.M., 1984, Tectonics and structural zonation of southern Tibet: Nature, v. 311, p. 219–223, doi: 10.1038/311219a0.

Burg, J.P., Guiraud, M., Chen, G.M., and Li, G.C., 1984, Himalayan metamorphism and deformations in the North Himalayan belt (Southern Tibet, China): Earth and Planetary Science Letters, v. 69, p. 391–400, doi: 10.1016/0012-821X(84)90197-3.

Burg, J.P., Nievergelt, P., Oberli, F., Seward, D., Davy, P., Maurin, J.C., Diao, Z.Z., and Meier, M., 1998, The Namche Barwa syntaxis: Evidence for exhumation related to compressional crustal folding: Journal of Asian Earth Sciences, v. 16, p. 239–252, doi: 10.1016/S0743-9547(98)00002-6.

Chemenda, A.I., Burg, J.P., and Mattauer, M., 2000, Evolutionary model of the Himalaya-Tibet system: Geopoem based on new modelling, geological and geophysical data: Earth and Planetary Science Letters, v. 174, p. 397–409, doi: 10.1016/S0012-821X(99)00277-0.

Chen, Z., Liu, Y., Hodges, K.V., Burchfiel, B.C., Royden, L.H., and Deng, C., 1990, The Kangmar Dome—A metamorphic core complex in Southern Xizang (Tibet): Science, v. 250, p. 1552–1556.

Coleman, M., and Hodges, K., 1995, Evidence for Tibetan Plateau uplift before 14-Myr Ago from a new minimum age for east-west extension: Nature, v. 374, p. 49–52, doi: 10.1038/374049a0.

de Sigoyer, J., Guillot, S., and Dick, P., 2004, Exhumation of the ultrahigh-pressure Tso Morari unit in eastern Ladakh (NW Himalaya): A case study: Tectonics, v. 23, no. TC3003, p. 1–18.

Dezes, P.J., Vannay, J.C., Steck, A., Bussy, F., and Cosca, M., 1999, Synorogenic extension: Quantitative constraints on the age and displacement of the Zanskar shear zone (northwest Himalaya): Geological Society of America Bulletin, v. 111, p. 364–374, doi: 10.1130/0016-7606(1999)111<0364:SEQCOT>2.3.CO;2.

Dodson, M.H., 1973, Closure temperature in cooling geochronological and petrological systems: Contributions to Mineralogy and Petrology, v. 40, p. 259–274, doi: 10.1007/BF00373790.

Donelick, R.A., Ketcham, R.A., and Carlson, W.D., 1999, Variability of apatite fission-track annealing kinetics: II, Crystallographic orientation effects: American Mineralogist, v. 84, p. 1224–1234.

Dubey, A.K., and Bhakuni, S.S., 2004, Development of extension faults on the oblique thrust ramp hanging wall: Example from the Tethys Himalaya: Journal of Asian Earth Sciences, v. 23, p. 427–434, doi: 10.1016/S1367-9120(03)00153-6.

Ehlers, T.A., Armstrong, P.A., and Chapman, D.S., 2001, Normal fault thermal regimes and the interpretation of low-temperature thermochronometers: Physics of the Earth and Planetary Interiors, v. 126, p. 179–194, doi: 10.1016/S0031-9201(01)00254-0.

England, P.C., and Richardson, S.W., 1977, The influence of erosion upon the mineral facies of rocks from different metamorphic environments: Geological Society [London] Journal, v. 134, p. 201–213.

England, P.C., and Thompson, A.B., 1984, Pressure temperature time paths of regional metamorphism, 1, Heat-transfer during the evolution of regions of thickened continental-crust: Journal of Petrology, v. 25, p. 894–928.

Frank, W., Grasemann, B., Guntli, P., and Miller, C., 1995, Geological map of the Kishtwar-Chamba-Kulu region (NW Himalayas, India): Vienna/A, Jahrbuch der Geologischen Bundesanstalt, v. 138, p. 299–308.

Fuchs, G., 1975, Contributions to the geology of the North-Western Himalayas: Vienna/A, Abhandlungen der Geologischen Bundesanstalt, v. 32, p. 59.

Fuchs, G., and Linner, M., 1996, On the geology of the suture zone and Tso Morari Dome in Eastern Ladakh (Himalaya): Vienna/A, Jahrbuch der Geologischen Bundesanstalt, v. 139, p. 191–207.

Gaetani, M., and Garzanti, E., 1991, Multicyclic history of the northern India continental margin (Northwestern Himalaya): American Association of Petroleum Geologists Bulletin, v. 75, p. 1427–1446.

Grujic, D., Casey, M., Davidson, C., Hollister, L.S., Kundig, R., Pavlis, T., and Schmid, S., 1996, Ductile extrusion of the Higher Himalayan Crystalline in Bhutan: Evidence from quartz microfabrics: Tectonophysics, v. 260, p. 21–43, doi: 10.1016/0040-1951(96)00074-1.

Gupta, V.J., and Kumar, S., 1975, Geology of Ladakh, Lahaul and Spiti regions of the Himalaya, with special reference to the stratigraphical position of the flysch deposits: Geologische Rundschau, v. 64, p. 540–563.

Hanmer, S., 1984, The potential use of planar and elliptical structures as indicators of strain regime and kinematics of tectonic flow: Geological Survey of Canada Paper, v. 84, p. 133–142.

Hayden, H.H., 1904, The geology of Spiti with parts of Bushahr and Rupshu: Geological Survey of India Memoir, v. 6, p. 1–121.

Herren, E., 1987, Zanskar Shear Zone—Northeast-southwest extension within the Higher Himalayas (Ladakh, India): Geology, v. 15, p. 409–413, doi: 10.1130/0091-7613(1987)15<409:ZSZNEW>2.0.CO;2.

Hodges, K.V., 1991, Pressure-temperature-time paths: Annual Review of Earth and Planetary Sciences, v. 19, p. 207–236, doi: 10.1146/annurev.ea.19.050191.001231.

Hodges, K.V., 2000, Tectonics of the Himalaya and southern Tibet from two perspectives: Geological Society of America Bulletin, v. 112, p. 324–350.

Hodges, K.V., and Silverberg, D.S., 1988, Thermal evolution of the Greater-Himalaya, Garwhal, India: Tectonics, v. 7, p. 583–600.

ISC, International Seismological Centre, 2004, On-line Bulletin, http://www.isc.ac.uk/Bull: Thatcham, UK.

John, B.E., and Foster, D.A., 1993, Structural and thermal constraints on the initiation angle of detachment faulting in the Southern Basin and Range—The Chemehuevi Mountains case study: Geological Society of America Bulletin, v. 105, p. 1091–1108, doi: 10.1130/0016-7606(1993)105<1091:SATCOT>2.3.CO;2.

Kapp, P., and Guynn, J.H., 2004, Indian punch rifts Tibet: Geology, v. 32, p. 993–996.

Ketcham, R.A., Donelick, R.A., and Carlson, W.D., 1999, Variability of apatite fission-track annealing kinetics: III, Extrapolation to geologic time scales: American Mineralogist, v. 84, p. 1235–1255.

Ketcham, R.A., Donelick, R.A., and Donelick, M.B., 2003, AFTSolve: A program for multi-kinetic modeling of apatite fission-track data: American Mineralogist, v. 88, p. 929.

Klootwijk, C.T., Conaghan, P.J., and Powell, C.M., 1985, The Himalayan arc—Large-scale continental subduction, oroclinal bending and back-arc spreading: Earth and Planetary Science Letters, v. 75, p. 167–183, doi: 10.1016/0012-821X(85)90099-8.

Kumar, A., Lal, N., Jain, A.K., and Sorkhabi, R.B., 1995, Late Cenozoic–Quaternary thermo-tectonic history of Higher Himalayan Crystalline (Hhc) in Kishtwar-Padar-Zanskar region, NW Himalaya—Evidence from fission-track ages: Journal of the Geological Society of India, v. 45, p. 375–391.

Lacassin, R., Valli, F., Arnaud, N., Leloup, P.H., Paquette, J.L., Haibing, L., Tapponier, P., Chevalier, M.-L., Guillot, S., Maheo, G., and Zhiqin, X., 2004, Large-scale geometry, offset and kinematic evolution of the Karakorum fault, Tibet: Earth and Planetary Science Letters, v. 219, p. 255–269, doi: 10.1016/S0012-821X(04)00006-8.

Lee, J., Hacker, B.R., Dinklage, W.S., Wang, Y., Gans, P., Calvert, A., Wan, J.L., Chen, W.J., Blythe, A.E., and McClelland, W., 2000, Evolution of the Kangmar Dome, southern Tibet: Structural, petrologic, and thermochronologic constraints: Tectonics, v. 19, p. 872–895, doi: 10.1029/1999TC001147.

Lee, J., Hacker, B., and Wang, Y., 2004, Evolution of North Himalayan gneiss domes: Structural and metamorphic studies in Mabja Dome, southern Tibet: Journal of Structural Geology, v. 26, p. 2297–2316, doi 10.1016/j.jsg.2004.02.013.

Lefort, P., 1975, Himalayas—Collided range—Present knowledge of continental arc: American Journal of Science, v. A275, p. 1.

Linker, M.F., Kirby, S.H., Ord, A., and Christie, J.M., 1984, Effects of compression direction on the plasticity and rheology of hydrolytically weakened synthetic quartz crystals at atmospheric-pressure: Journal of Geophysical Research, v. 89, p. 4241–4255.

Maheo, G., Guillot, S., Blichert-Toft, J., Rolland, Y., and Pecher, A., 2002, A slab breakoff model for the Neogene thermal evolution of South Karakorum and South Tibet: Earth and Planetary Science Letters, v. 195, p. 45–58, doi: 10.1016/S0012-821X(01)00578-7.

Mancktelow, N.S., and Pavlis, T.L., 1994, Fold-fault relationships in low-angle detachment systems: Tectonics, v. 13, p. 668–685, doi: 10.1029/93TC03489.

McCaffrey, R., and Nabelek, J., 1998, Role of oblique convergence in the active deformation of the Himalayas and southern Tibet plateau: Geology, v. 26, p. 691–694, doi: 10.1130/0091-7613(1998)026<0691:ROOCIT>2.3.CO;2.

McDougall, I., and Harrison, T.M., 1999, Geochronology and thermochronology by the ^{40}Ar/^{39}Ar method (2nd edition): New York, Oxford University Press, 269 p.

Mohindra, R., and Bagati, T.N., 1996, Seismically induced soft-sediment deformation structures (seismites) around Sumdo in the lower Spiti valley (Tethys Himalaya): Sedimentary Geology, v. 101, p. 69–83, doi: 10.1016/0037-0738(95)00022-4.

Molnar, P., and Chen, W.P., 1983, Focal depths and fault plane solutions of earthquakes under the Tibetan Plateau: Journal of Geophysical Research, v. 88, p. 1180–1196.

Molnar, P., and Lyon-Caen, H., 1989, Fault plane solutions of earthquakes and active tectonics of the Tibetan Plateau and its margins: Geophysical Journal International, v. 99, p. 123–153.

Molnar, P., and Tapponnier, P., 1975, Cenozoic tectonics of Asia—Effects of a continental collision: Science, v. 189, p. 419–426.

Molnar, P., and Tapponnier, P., 1978, Active tectonics of Tibet: Journal of Geophysical Research, v. 83, p. 5361–5375.

Murphy, M.A., and Copeland, P., 2005, Transtensional deformation in the central Himalaya and its role in accommodating growth of the Himalayan orogen: Tectonics, v. 24, no. 4, p. TC4012.

Murphy, M.A., Yin, A., Kapp, P., Harrison, T.M., Manning, C.E., Ryerson, F.J., Ding, L., and Guo, J.H., 2002, Structural evolution of the Gurla Mandhata detachment system, southwest Tibet: Implications for the eastward extent of the Karakoram fault system: Geological Society of America Bulletin, v. 114, p. 428–447, doi: 10.1130/0016-7606(2002)114<0428:SEOTGM>2.0.CO;2.

Nelson, K.D., Zhao, W.J., Brown, L.D., Kuo, J., Che, J.K., Liu, X.W., Klemperer, S.L., Makovsky, Y., Meissner, R., Mechie, J., Kind, R., Wenzel, F., Ni, J., Nabelek, J., Chen, L.S., Tan, H.D., Wei, W.B., Jones, A.G., Booker, J., Unsworth, M., Kidd, W.S.F., Hauck, M., Alsdorf, D., Ross, A., Cogan, M., Wu, C.D., Sandvol, E., and Edwards, M., 1996, Partially molten middle crust beneath southern Tibet: Synthesis of project INDEPTH results: Science, v. 274, p. 1684–1688, doi: 10.1126/science.274.5293.1684.

Ni, J., and Barazangi, M., 1984, Seismotectonics of the Himalayan collision zone—Geometry of the underthrusting Indian plate beneath the Himalaya: Journal of Geophysical Research, v. 89, p. 1147–1163.

Ni, J., and Barazangi, M., 1985, Active tectonics of the western Tethyan Himalaya above the underthrusting Indian plate—The Upper Sutlej River Basin as a pull-apart structure: Tectonophysics, v. 112, p. 277–295, doi: 10.1016/0040-1951(85)90183-0.

Ni, J., and York, J.E., 1978, Late Cenozoic tectonics of Tibetan Plateau: Journal of Geophysical Research, v. 83, p. 5377–5384.

Pan, Y., Copeland, P., Roden, M.K., Kidd, W.S.F., and Harrison, T.M., 1993, Thermal and unroofing history of the Lhasa area, Southern Tibet—Evidence from apatite fission-track thermochronology: Nuclear Tracks and Radiation Measurements, v. 21, p. 543–554, doi: 10.1016/1359-0189(93)90195-F.

Passchier, C.W., and Simpson, C., 1986, Phorphyroclast systems as kinematic indicators: Journal of Structural Geology, v. 8, p. 831–844, doi: 10.1016/0191-8141(86)90029-5.

Phillips, R.J., Parrish, R.R., and Searle, M.P., 2004, Age constraints on ductile deformation and long-term slip rates along the Karakoram fault zone, Ladakh: Earth and Planetary Science Letters, v. 226, p. 305–319, doi: 10.1016/j.epsl.2004.07.037.

Purdy, J.E., and Jaeger, E., 1976, K-Ar ages on rock-forming minerals from the Central Alps: Padova, Memory of the Institute of Geology and Mineralogy, University of Padova, v. 30, p. 1–32.

Qiang, X.K., Li, Z.X., Powell, C.M., and Zheng, H.B., 2001, Magnetostratigraphic record of the late Miocene onset of the East Asian monsoon, and Pliocene uplift of northern Tibet: Earth and Planetary Science Letters, v. 187, p. 83–93, doi: 10.1016/S0012-821X(01)00281-3.

Quidelleur, X., Grove, M., Lovera, O.M., Harrison, T.M., Yin, A., and Ryerson, F.J., 1997, Thermal evolution and slip history of the Renbu Zedong Thrust, southeastern Tibet: Journal of Geophysical Research—Solid Earth, v. 102, p. 2659–2679, doi: 10.1029/96JD02483.

Ramsay, J.G., 1967, Folding and fracturing of rocks: New York, McGraw Hill, 568 p.

Ramsay, J.G., and Huber, M.I., 1987, Techniques of modern structural geology, Vol. 2: Folds and fractures: London, Academic Press, 700 p.

Ratschbacher, L., Frisch, W., Liu, G.H., and Chen, C.S., 1994, Distributed deformation in southern and western Tibet during and after the India-Asia collision: Journal of Geophysical Research—Solid Earth, v. 99, p. 19,917–19,945, doi: 10.1029/94JB00932.

Rey, P., Vanderhaeghe, O., and Teyssier, C., 2001, Gravitational collapse of the continental crust: Definition, regimes and modes: Tectonophysics, v. 342, p. 435–449, doi: 10.1016/S0040-1951(01)00174-3.

Robyr, M., Vannay, J.C., Epard, J.L., and Steck, A., 2002, Thrusting, extension, and doming during the polyphase tectonometamorphic evolution of the High Himalayan Crystalline Zone in NW India: Journal of Asian Earth Sciences, v. 21, p. 221–239, doi: 10.1016/S1367-9120(02)00039-1.

Royden, L., 1996, Coupling and decoupling of crust and mantle in convergent orogens: Implications for strain partitioning in the crust: Journal of Geophysical Research—Solid Earth, v. 101, p. 17,679–17,705, doi: 10.1029/96JB00951.

Royden, L.H., and Burchfiel, B.C., 1987, Thin-skinned north-south extension within the convergent Himalayan region: Gravitational collapse of a Miocene topographic front: Geological Society [London] Special Publication 28, p. 611–619.

Schlup, M., Carter, A., Cosca, M., and Steck, A., 2003, Exhumation history of eastern Ladakh revealed by Ar-40/Ar-39 and fission-track ages: The Indus River–Tso Morari transect, NW Himalaya: Geological Society [London] Journal, v. 160, p. 385–399.

Schneider, D.A., Edwards, M.A., Kidd, W.S.F., Asif Khan, M., Seeber, L., and Zeitler, P.K., 1999, Tectonics of Nanga Parbat, western Himalaya; synkinematic plutonism within the doubly vergent shear zones of a crustal-scale pop-up structure: Geology, v. 27, p. 999–1002, doi: 10.1130/0091-7613(1999)027<0999:TONPWH>2.3.CO;2.

Searle, M.P., Weinberg, R.F., and Dunlap, W.J., 1998, Transpressional tectonics along the Karakoram fault zone, northern Ladakh: Constraints on Tibetan extrusion, *in* Holdsworth, R.E., Strachan, R.A., and Dewey, J.F., eds., Continental Transpressional and Transtensional Tectonics: Geological Society [London] Special Publication 135, p. 307–326.

Singh, S., Sinha, P., Jain, A.K., Singh, V.N., and Srivastava, L.S., 1975, Preliminary report on the January 19, 1975, Kinnaur earthquake in Himachal Pradesh: Earthquake Engineering Studies, v. 75, p. 1–32.

Spicer, R.A., Harris, N.B.W., Widdowson, M., Herman, A.B., Guo, S.X., Valdes, P.J., Wolfe, J.A., and Kelley, S.P., 2003, Constant elevation of southern Tibet over the past 15 million years: Nature, v. 421, p. 622–624, doi: 10.1038/nature01356.

Steck, A., 2003, Geology of the NW Indian Himalaya: Eclogae Geologicae Helvetiae, v. 96, no. 2, p. 147–196.

Steck, A., Spring, L., Vannay, J.C., Masson, H., Stutz, E., Bucher, H., Marchant, R., and Tieche, J.C., 1993, Geological transect across the northwestern Himalaya in eastern Ladakh and Lahul (a model for the continental collision of India and Asia): Eclogae Geologicae Helvetiae, v. 86, p. 219.

Steck, A., Epard, J.L., Vannay, J.C., Hunziker, J., Girard, M., Morard, A., and Robyr, M., 1998, Geological transect across the Tso Morari and Spiti areas: The nappe structures of the Tethys Himalaya: Eclogae Geologicae Helvetiae, v. 91, p. 103–122.

Stephenson, B.J., Waters, D.J., and Searle, M.P., 2000, Inverted metamorphism and the main central thrust: Field relations and thermobarometric constraints from the Kishtwar Window, NW Indian Himalaya: Journal of Metamorphic Geology, v. 18, p. 571–590, doi: 10.1046/j.1525-1314.2000.00277.x.

Tapponnier, P., and Molnar, P., 1977, Active faulting and tectonics in China: Journal of Geophysical Research, v. 82, p. 2905–2930.

Taylor, M., Yin, A., Ryerson, F.J., Kapp, P., and Ding, L., 2003, Conjugate strike-slip faulting along the Bangong-Nujiang suture zone accommodates coeval east-west extension and north-south shortening in the interior of the Tibetan Plateau: Tectonics, v. 22, article no. 1044.

Thiede, R., Bookhagen, B., Arrowsmith, J.R., Sobel, E., and Strecker, M., 2004, Climatic control on rapid exhumation along the Southern Himalayan Front: Earth and Planetary Science Letters, v. 222, p. 791–806, doi: 10.1016/j.epsl.2004.03.015.

Tullis, J., and Yund, R.A., 1987, Transition from cataclastic flow to dislocation creep of feldspar—Mechanisms and microstructures: Geology, v. 15, p. 606–609, doi: 10.1130/0091-7613(1987)15<606:TFCFTD>2.0.CO;2.

Vanderhaeghe, O., Teyssier, C., and Wysoczanski, R., 1999, Structural and geochronological constraints on the role of partial melting during the formation of the Shuswap metamorphic core complex at the latitude of the Thor-Odin dome, British Columbia: Canadian Journal of Earth Sciences, v. 36, p. 917–943, doi: 10.1139/cjes-36-6-917.

Vannay, J.C., Grasemann, B., Rahn, M., Frank, W., Carter, A., and Baudraz, V., 2004, Miocene to Holocene exhumation of metamorphic crustal wedges in the Himalayan orogen: Evidence for tectonic extrusion coupled to fluvial erosion: Tectonics, v. 23, p. TC1014.

Watts, D.R., and Harris, N.B.W., 2005, Mapping granite and gneiss in domes along the North Himalayan antiform with ASTER SWIR band ratios: Geological Society of America Bulletin, v. 117, p. 879–886, doi: 10.1130/B25592.1.

Wiesmayr, G., and Grasemann, B., 2002, Eohimalayan fold and thrust belt: Implications for the geodynamic evolution of the NW-Himalaya (India): Tectonics, v. 21, article no. 1058.

Yin, A., and Harrison, T.M., 2000, Geologic evolution of the Himalayan-Tibetan orogen: Annual Review of Earth and Planetary Sciences, v. 28, p. 211–280, doi: 10.1146/annurev.earth.28.1.211.

Yin, A., Harrison, T. M., Ryerson, F. J., Chen, W.J., Kidd, W.S.F., and Copeland, P., 1994, Tertiary structural evolution of the Gangdese thrust system, southeastern Tibet: Journal of Geophysical Research—Solid Earth, v. 99, p. 18,175–18,201, doi: 10.1029/94JB00504.

Yin, A., Harrison, T.M., Murphy, M.A., Grove, M., Nie, S., Ryerson, F.J., Feng, W.X., and Le, C.Z., 1999a, Tertiary deformation history of southeastern and southwestern Tibet during the Indo-Asian collision: Geological Society of America Bulletin, v. 111, p. 1644–1664, doi: 10.1130/0016-7606(1999)111<1644:TDHOSA>2.3.CO;2.

Yin, A., Kapp, P.A., Murphy, M.A., Manning, C.E., Mark Harrison, T., Grove, M., Lin, D., Xi-Guang, D., and Cun-Ming, W., 1999b, Significant late Neogene east-west extension in northern Tibet: Geology, v. 27, p. 787–790, doi: 10.1130/0091-7613(1999)027<0787:SLNEWE>2.3.CO;2.

Zhang, P., Molnar, P., and Downs, W.R., 2001, Increased sedimentation rates and grain sizes 2–4 Myr ago due to the influence of climate change on erosion rates: Nature, v. 410, p. 891–897.

Manuscript Received by the Society 15 July 2005
Revised Manuscript Received 17 January 2006
Manuscript Accepted 27 January 2006

Printed in the USA